nature geoscience

LETTERS

PUBLISHED ONLINE: 13 SEPTEMBER 2009 | DOI: 10.1038/NGEO622

No asymmetry in geomagnetic reversals recorded by 1.1-billion-year-old Keweenawan basalts

Nicholas L. Swanson-Hysell[1]*, Adam C. Maloof[1], Benjamin P. Weiss[2] and David A. D. Evans[3]

Interpreting the past latitude and geography of the continents from palaeomagnetic data relies on the key assumption that Earth's geomagnetic field behaves as a geocentric axial dipole. The axial dipolar field model implies that all geomagnetic reversals should be symmetric. However, palaeomagnetic data from volcanic rocks produced by the 1.1-billion-year-old Keweenawan Rift system in North America have been interpreted to show asymmetric reversals, which had led to the suggestion that there was a significant non-axial dipole contribution to the magnetic field during this time[1,2]. Here we present high-resolution palaeomagnetic data that span three geomagnetic field reversals from a well-described series of basalt flows at Mamainse Point, Ontario, in the Keweenawan Rift. Our data show that each reversal is symmetric. We thus conclude that the previously documented reversal asymmetry is an artefact of the rapid motion of North America during this time. Comparisons of reversed and normal populations that were time-averaged over entire polarity intervals, or from sites not directly on either side of a geomagnetic reversal, have previously led to the appearance of reversal asymmetry.

Extrusive and intrusive igneous rocks of the Keweenawan province form part of a failed mid-continent rift (MCR) system that was active from 1.11 to 1.09 Gyr ago. The largest areal exposure of these rocks is in the Lake Superior region, but aeromagnetic and gravity surveys show that the relatively dense and magnetic volcanic rocks of the rift span more than 3,000 km, largely beneath sedimentary cover (Fig. 1)[3]. Palaeomagnetic data from Keweenawan rocks have been compiled to generate an apparent polar wander (APW) path for North America, known as the Logan Loop[4–6]. Comparisons of the Logan Loop with APW paths from other continents have been used to reconstruct the supercontinent Rodinia[7,8].

Palaeomagnetic directions from MCR rocks consistently reveal normal and reversed directions that are not antiparallel (with inclination differences of 20°–30°; Fig. 1)[4]. This pattern has been interpreted as reversal asymmetry, leading to speculation that significant non-dipole components may have contributed to the surface geomagnetic field[1,2]. The well-known problem of Keweenawan reversal asymmetry is often cited as an uncertainty in palaeogeographic reconstructions[7–9], as the introduction of quadrupole and octupole components to the geomagnetic field can lead to significant discrepancies between true palaeolatitude and palaeomagnetically derived palaeolatitude[10]. Much of the movement of the late Mesoproterozoic APW path for Laurentia occurs across what has been interpreted as an 'asymmetric' reversal. The large magnitude of this apparent motion makes it important to understand whether the difference in inclination between normal and reversed directions is an artefact of a significant non-dipole contribution to the field, or whether it is due to motion of the North American continent. This information is critical for deciphering North American plate motions during the Himalayan-scale Grenville Orogeny and the assembly of cratons to form the supercontinent Rodinia. A better understanding of the late Mesoproterozoic geomagnetic field is also necessary to evaluate claims of non-uniformitarian processes in the Proterozoic era, such as true polar wander and low-latitude glaciation, which rely on the uniformitarian geocentric axial dipole (GAD) hypothesis[11,12].

Previous studies have compared the mean of all Keweenawan-aged reversed directions with all normal directions[2,4] and/or have grouped all reversed and normal directions at a single study location[13,14]. To fully evaluate whether the actual reversals are asymmetric, it is essential to obtain high-resolution palaeomagnetic data through stratigraphic sampling that spans reversals in the context of detailed volcanostratigraphy.

The basalt flows at Mamainse Point unconformably overlie the Archaean Superior Province on the northeastern shore of Lake Superior (Fig. 1) and represent the most complete record of extrusive Keweenawan volcanism. Mamainse Point is the only known locality in the MCR where multiple reversals are recorded in a succession of extrusive lava flows, as there are three reversals (reversed → normal → reversed → normal) throughout the ∼4,500 m of basalt flows and inter-rift sediments.

Here we report palaeomagnetic data from 73 basalt flows at Mamainse Point that span the three reversals at high resolution and show each reversal to be symmetric (Fig. 2). There is a progressive decrease in the inclination of the palaeomagnetic data up-stratigraphy from ∼70° to ∼30° that we interpret as resulting from the equatorward movement of Laurentia. As a result of this progressive change in palaeolatitude through time, a reversal test that uses means of entire polarity zones may result in a false negative.

Palaeomagnetic studies at other localities in the MCR have revealed a general pattern that older rocks carry a reversed magnetization and younger rocks record a normal magnetization (Fig. 1c; Supplementary Table S3). This trend led early workers to postulate that there was only one geomagnetic reversal during the 11 Myr of Keweenawan volcanism and that this reversal could be used as a stratigraphic datum for all Keweenawan igneous units[5,13–15]. When Palmer[13] discovered multiple reversals in the sequence of basalts at Mamainse Point, this single-reversal paradigm led him to propose the presence of a sequence-repeating fault, despite the fact that, in his words, there is 'no geological evidence to support the fault hypothesis'. In addition to the lack of geological evidence, the fault repetition hypothesis has been discounted by geochemical data (Fig. 2b; see Supplementary Information for a more complete description of previous palaeomagnetic work at Mamainse Point and other dual-polarity localities in the MCR)[16].

[1]Department of Geosciences, Princeton University, Guyot Hall, Washington Road, Princeton, New Jersey 08544, USA, [2]Department of Earth, Atmospheric and Planetary Sciences, Massachusetts Institute of Technology, 77 Massachusetts Avenue, Cambridge, Massachusetts 02139, USA, [3]Department of Geology and Geophysics, Yale University, 210 Whitney Avenue, New Haven, Connecticut 06520, USA. *e-mail: nswanson@princeton.edu.

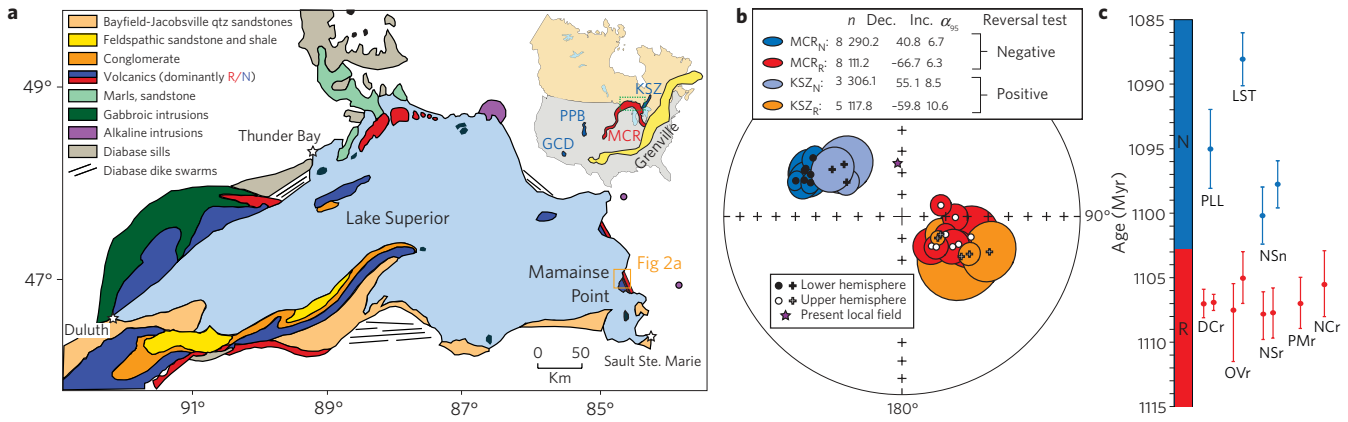

Figure 1 | Mid-continent rift geology and palaeomagnetic data. a, Generalized geologic map of the Lake Superior region after Halls and Pesonen[4]. The inset map shows the location of the mid-continent rift (MCR) gravity anomaly, the Kapuskasing structural zone (KSZ), the Pikes Peak batholith (PPB) and the Gila County diabases (GCD). **b**, Equal-area plot of tilt-corrected polarity zone means and α_{95} error ellipses from all MCR dual-polarity locales. MCR data (red and dark blue) show 20°–40° of inclination asymmetry and fail a reversal test, whereas KSZ directions (orange and light blue) pass a reversal test. **c**, U/Pb ages with 2σ error bars from locations with both palaeomagnetic and geochronological data (see Supplementary Table S3 and ref. 15). DCr: Duluth Complex reversed, LST: Lake Shore Traps, NCr: Nemegosenda Carbonatite normal, NSn: North Shore Volcanics normal, NSr: North Shore reversed, OVr: Osler Volcanics reversed, PLL: Portage Lake Lavas, PMr: Powder Mill Volcanics.

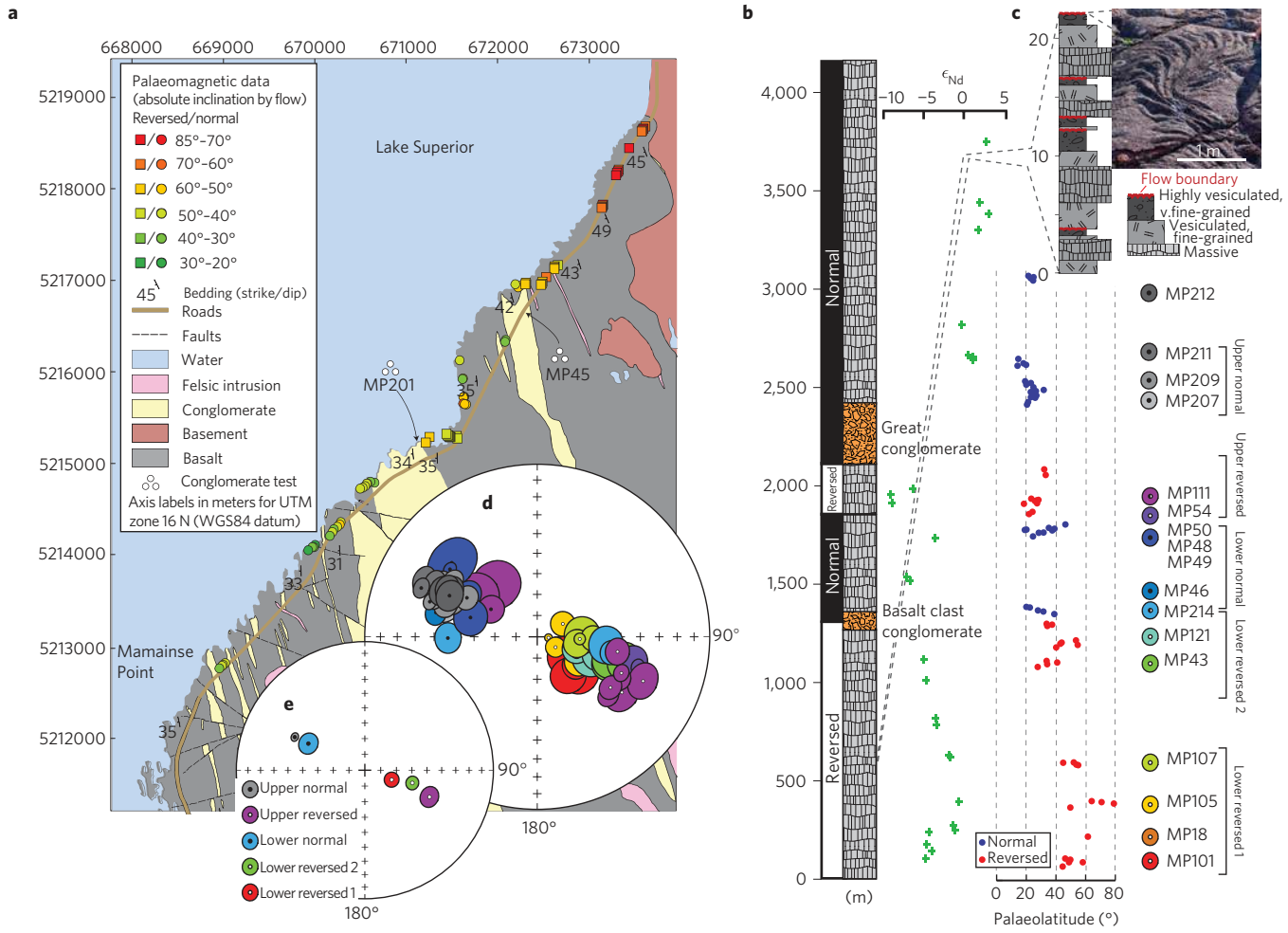

Figure 2 | Summary of palaeomagnetic data from Mamainse Point. a, Geological map of Mamainse Point[30] with a symbol at each flow with palaeomagnetic data (colour-coded by magnetic inclination with squares for reversed and circles for normal). **b**, Simplified stratigraphy with ϵ_{Nd} data[16] and absolute palaeolatitude for the virtual geomagnetic pole (VGP) of each flow. **c**, Stratigraphy for basalt flows from the MP107 section with a photo of a pahoehoe flow top. **d**, Equal-area plot of the tilt-corrected Fisher mean and associated α_{95} ellipse for each flow sampled—colours correspond to individual sections shown in stratigraphic position in **b**. **e**, Equal-area plot of tilt-corrected Fisher means of flow VGPs grouped as indicated by the right-most brackets in **b**.

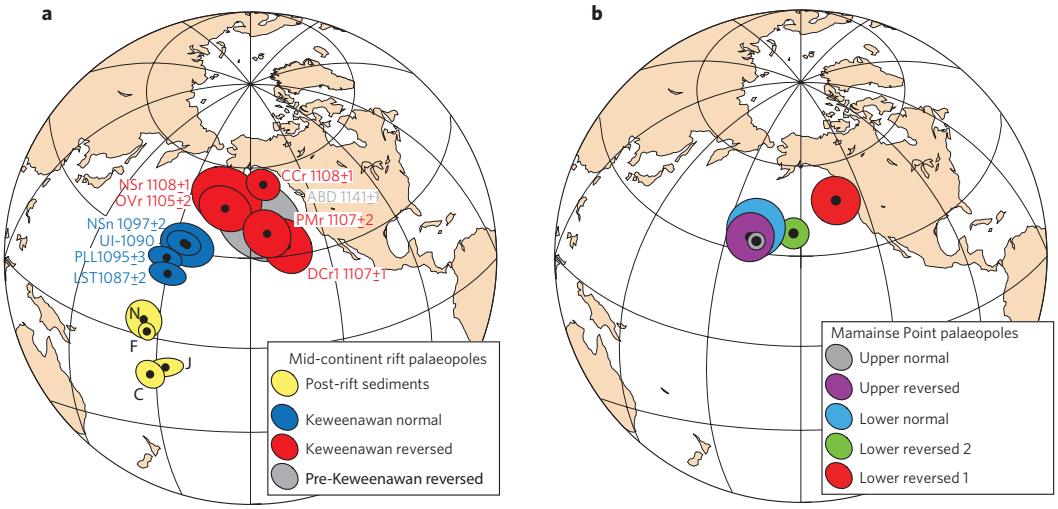

Figure 3 | The Logan Loop and Mamainse Point poles. a, Equal-area projection of poles for all MCR volcanics for which there are both palaeomagnetic and geochronological data (see Supplementary Table S3). ABD: Abitibi Dykes, CCr: Coldwell Complex reversed. The yellow palaeopoles are from rift sediments deposited after the cessation of volcanism but do not have rigorous geochronological control. Their relative deposition is such that from oldest to youngest: N → F → J → C. N: Nonesuch Shale, F: Freda Sandstone, J: Jacobsville Sandstone, C: Chequamegon Sandstone. **b**, Palaeopoles from the Mamainse Point succession calculated using the mean of flow VGPs as grouped in Fig. 2 (see Supplementary Table S2 for palaeopole parameters).

Further evidence of multiple reversals during MCR volcanism comes from coeval alkaline complexes exposed along the Kapuskasing structural zone (Fig. 1). At least three of these alkaline complexes contain nearly symmetric polarity reversals. Whereas some record a reversed to normal polarity change, others record a change from normal to reversed[17]. One of these units, the Coldwell Complex, represents at least three intrusive episodes. Although the determination of cross-cutting relationships can be difficult owing to complex cooling histories, palaeomagnetic data from the Coldwell Complex are interpreted to reflect a R1 → N → R2 polarity history with only 5°–10° of inclination asymmetry between reversals (Fig. 1b; Supplementary Table S3)[18].

Owing to the progressive decrease in the inclination of the magnetization upwards through the stratigraphy at Mamainse Point (Fig. 2), a reversal test[19] on the new data set that compares all reversed directions with all normal ones fails, consistent with the previous literature. However, if the three reversals are considered individually, each one passes a reversal test. The first reversal occurs during a hiatus in volcanism and the deposition of the basalt clast conglomerate. A reversal test comparing the three reversed flows below the conglomerate in section MP214 to the three normal flows of MP214 above is positive with a 'B' classification ($\gamma_c = 10.0$). This test shows that the angle between reversed and normal populations (γ_o) is less than the angle at which the null hypothesis of a common mean direction would be rejected with 95% confidence (γ_c) and because γ_c is between 5° and 10° it is given a 'B' classification. The flows above the basalt clast conglomerate are normally magnetized and lead up to flows of reversed magnetization without separation by a conglomerate. Three of the flows have anomalous declinations and could possibly be transitional. A reversal test conducted between all of the flows in the lower normal polarity zone (11 flows) and all of the flows in the upper reversed polarity zone (10 flows) passes with a 'B' classification ($\gamma_c = 9.8$). The uppermost reversal occurs within the 'great conglomerate'. A reversal test between all of the flows of the upper reversed zone and the 13 normal flows of sections MP207 and MP209 above the conglomerate is positive with a 'B' classification ($\gamma_c = 6.1$).

A fundamental assumption of many palaeomagnetic studies is that the surface expression of the geomagnetic field behaves as a time-averaged GAD, where mean field inclination (I) is a simple function of latitude ($\tan(I) = 2\tan(\lambda)$). Under the GAD hypothesis, palaeomagnetic data that span enough time to average out secular variation should produce a palaeomagnetic pole that corresponds to Earth's spin axis. Archaeomagnetic studies show that, over the past 10,000 years, Earth's magnetic field is best described by a GAD (ref. 20). Palaeomagnetic data are broadly consistent with a GAD for the past 100–150 Myr (the only period for which reliable plate reconstructions can be made independent of palaeomagnetic data) with only a small (3–5%) axial quadrupole component[21]. Palaeolatitude calculations made assuming a GAD geomagnetic field correspond well with climatic indicators of latitude, such as evaporite basins, for the past 2 Gyr (ref. 22).

The interpreted reversal asymmetry in Keweenawan data sets led Pesonen and Nevanlinna[1,2] to propose that the ~1.1 Gyr geomagnetic field contained significant non-dipole components. Specifically, Pesonen and Nevanlinna proposed that in addition to the main dipole there was a persistent offset dipole. They argued that 'reversal asymmetry' resulted from the main dipole reversing while the offset dipole retained constant polarity. This contribution to the geomagnetic field can alternatively be expressed in terms of zonal harmonics as a geocentric dipole (g_1^0) and an axial quadrupole (g_2^0) where the reversal asymmetry results from a reversing dipole and a non-reversing quadrupole. Reversal asymmetry would also arise if there was a significant axial octupole (g_3^0), or any other higher-order component, that maintained constant polarity during the reversal of the dipole.

Another approach for evaluating the GAD hypothesis has been to calculate the elongation parameter for palaeomagnetic data sets from periods of rapid volcanism when the host continent can be assumed to be effectively stationary[23]. The resulting elongation/inclination data pairs can then be compared with statistical models of palaeosecular variation that predict the distribution of geomagnetic field vectors for a GAD and thus a single elongation value for each inclination. For the Mamainse Point data presented herein, the applicability of this method is limited because the necessary condition of a stationary continent for an interval in which 100 flows can be sampled cannot be met owing to the significant change in palaeolatitude through the section. Although it is possible that there is a locality within the rift where high rates of volcanism could yield flows that effectively meet the stationary criteria, the fast rates of APW through the interval (Fig. 3) will probably complicate this analysis in most localities.

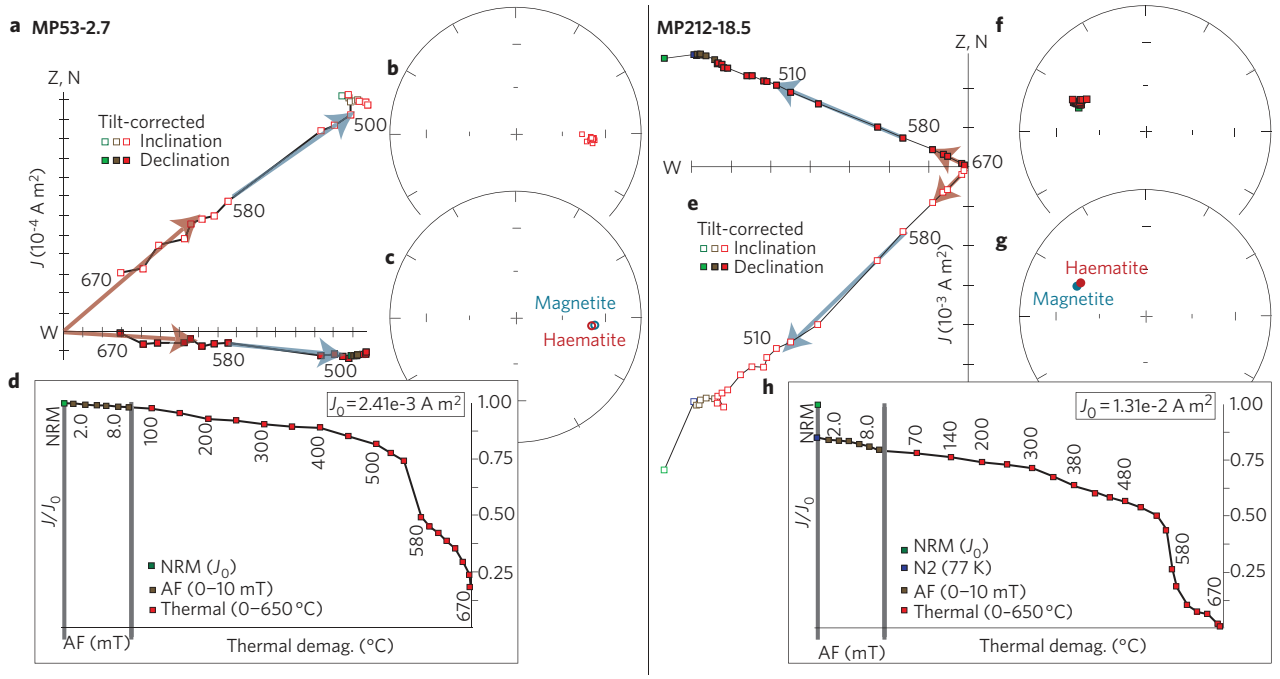

Figure 4 | Example palaeomagnetic data. a–h, Representative vector-component (Zijderveld) diagrams (**a** and **e**), equal-area projections (**b** and **f**), least-squares fits (**c** and **g**) and magnetic intensity (J/J_0) plots (**d** and **h**) for Mamainse Point basalts. In the vector-component plots, the haematite fit is traced with a red arrow and the magnetite fit is traced with a blue arrow. These components are summarized in equal-area plots (**c** and **g**). In all plots, green-filled squares are natural remanent magnetization (NRM), brown-filled squares are alternating field (AF) demagnetization steps and red-filled squares reflect thermal demagnetization. In the equal-area plots (**b** and **f**), colour-filled/colour-rimmed circles represent lower/upper-hemisphere directions. All data are in tilt-corrected coordinates.

As the three reversals in the succession at Mamainse Point are symmetric, there is no need to invoke substantial deviations from a GAD such as a non-reversing quadrupole or octupole. Although this result does not preclude non-dipole contributions to the geomagnetic field during the Mesoproterozoic era, it does eliminate the main rationale that has been used to question the validity of the GAD hypothesis during the time period. This rationale is further weakened by the presence of symmetric reversals in 1.4 Gyr sedimentary red beds[24] and in carbonates of Mesoproterozoic age[25]. Instead of resulting from reversal asymmetry, the change in inclination observed through the succession is readily explained as a consequence of continental motion.

Palaeomagnetic poles that are paired with U–Pb geochronological data constrain the rate of continental motion during Keweenawan volcanism (Fig. 3). A comparative analysis of palaeopoles suggests that the volcanism at Mamainse Point spans much of the period of Keweenawan volcanism given the similarity of the 'lower reversed 1' pole to the Coldwell Complex reversed 1 pole, which has an age of 1,108 ± 1 Myr and the similarity of the 'upper normal' pole to the North Shore Volcanics normal pole, which has an age of 1,097 ± 2 Myr. Using the conclusion that the field was probably a GAD, we can calculate the minimum velocity that is implied by the motion from the Coldwell Complex reversed 1 pole to the North Shore Volcanics normal pole to be 33.6 ± 3.5 cm yr^{-1} (see Supplementary Information for error calculation methods and Supplementary Table S4 for rates between all Keweenawan palaeomagnetic poles with U/Pb ages). The estimates for the rate of motion from 1,108 Myr to 1,094 Myr range between 21.5 ± 7.1 cm yr^{-1} for Osler Volcanics reversed → North Shore normal, to 38.5 ± 4.4 cm yr^{-1} for Duluth Complex reversed → North Shore normal. The compilation of polar wander rates shows that during later Keweenawan volcanism movement slowed (as has previously been noted by Davis and Green[26]). The rate from the 1,097 Myr North Shore normal pole to the 1,087 Myr Lake Shore Trap pole is 12.2 ± 6.4 cm yr^{-1}. These rates for the motion of North America during the first 10 million years of Keweenawan volcanism are faster than the modelled speed limit of 20 cm yr^{-1} for plate tectonic motions imposed by bending stresses associated with the subduction of oceanic lithosphere[27]. The only plate to reach this theoretical limit during the past 150 Myr was India as it travelled north following the break-up of Gondwanaland. Either 20 cm yr^{-1} is not a firm speed limit for plate motion at 1 Gyr, or some of the motion observed could be a result of true polar wander that drove the North American continent and the mid-continent rift, towards the equator at rates slightly faster than those of plate tectonics[28]—a possibility that could be tested with data from other continents.

The period of Keweenawan volcanism was a time of significant equatorward motion of the North American continent. As a result of this progressive change in palaeolatitude, previous reversal tests that used means from combined results in each polarity produced false negatives. Detailed stratigraphic context combined with high-resolution data are essential for understanding both the behaviour of the geomagnetic field and APW paths in the late Mesoproterozoic era.

Methods

The extrusive basalt flows at Mamainse Point are remarkably preserved and range from less than 1 m to more than 20 m thick. Individual flows usually follow this general stratigraphy from base to top: (1) massive (relatively coarse-grained) with scattered elongate-upwards pipe vesicles (see Supplementary Fig. S12), (2) massive with occasionally apparent flow banding, (3) massive with some vesicles, (4) highly vesiculated and fine-grained and (5) flow tops often with pahoehoe textures and slight ferruginization (Fig. 2c; see Supplementary Figs S9–S11 for further photos of the basalts). Individual flows and sedimentary hiatuses can be delineated, allowing us to place our palaeomagnetic sampling in a robust stratigraphic context. Although there are numerous conglomerates interbedded with the flows particularly in the upper portion of the stratigraphy (Fig. 2a), there are two especially thick conglomerates. The lower of these is the 'basalt clast conglomerate', which is contained within our section MP214 where the

conglomerate is 39 m thick. The upper conglomerate, or 'great conglomerate', is ~310 m thick and shows a progressive increase in the percentage of clasts derived from Superior Province basement relative to basalt clasts (see clast counts in Supplementary Fig. S8).

Multiple samples (usually 5–6) were collected and subsequently analysed from 73 flows spanning the stratigraphy from the lower contact with the Superior Province metamorphic rocks to above the third reversal in the succession (see Supplementary Information for a description of the detailed demagnetization routines used). The thermal demagnetization behaviour and hysteresis loops of the basalt samples (Fig. 4 and Supplementary Fig. S1,S2 and S4–S7) show that the magnetization is carried by both haematite and magnetite. Whereas the magnetite exists as a primary igneous mineral in the basalt, the haematite probably formed as a result of deuteritic oxidation shortly after the eruption of each flow. Our detailed thermal demagnetization protocol allows for comparison of the haematite and magnetite components. Our data demonstrate that the characteristic magnetization components carried by the two mineralogies (unblocked between 500 and 575 °C for magnetite and 650–675 °C for haematite) are consistently of a very similar direction (Fig. 4). This result suggests that the haematite formed during initial cooling of the basalts or during pedogenesis that occurred soon after flow emplacement and recorded the same snapshot of the geomagnetic field as the magnetite component. In some instances, the high intensity of the haematite component prevented isolation of the magnetite component. For 16 flows, it was therefore necessary to use the haematite component as the characteristic remanent magnetization (ChRM) and for an extra 12 flows magnetite fits were used for some samples and haematite for others, as indicated in Supplementary Table S1. When a magnetite component was confidently isolated, as indicated by a 'shoulder' in plots of J/J_0, a least-squares fit through the demagnetization steps in its unblocking range was used as the ChRM (see Supplementary Table S1 for the mean direction of each flow). A number of flows have an extra magnetization component that unblocks between 590 and 650 °C that is of opposite polarity to the components that unblock between 500 and 575 °C and between 650 and 675 °C (see Supplementary Fig. S2) and is further discussed in Supplementary Information. Fisher means were calculated for each flow from the ChRM directions isolated through principal component analysis[29] of samples within that flow (Supplementary Table S1).

Clasts were sampled and analysed from the basalt clast conglomerate (site MP45; Supplementary Fig. S11) and from basalt clasts within the great conglomerate (site MP201; Supplementary Fig. S11) allowing for two conglomerate tests (see Supplementary Fig. S3). Least-squares fits to both the magnetite and haematite components for each test are consistent with selection from a random population (see Supplementary Information for details of the test results). These conglomerate test results further confirm that both the magnetite and haematite components observed in the flows were acquired before the erosion of the flows and the deposition of these conglomerates that were deposited within the larger stack of Keweenawan basalts. Therefore, we can be confident in the use of these directions as a record of the local magnetic field at the time the flows erupted and cooled.

The terms 'normal' and 'reversed' when applied to palaeomagnetic directions from the MCR are not intended to specify the absolute orientation of the geomagnetic field at the time of volcanism, as there are unresolved parts of the APW path for Laurentia since the Mesoproterozoic era. Rather, the designation distinguishes between directions with negative inclinations (reversed) and directions with positive inclinations (normal), a convention used in all previous palaeomagnetic studies of Keweenawan volcanics.

Received 22 April 2009; accepted 5 August 2009; published online 13 September 2009

References

1. Pesonen, L. & Nevanlinna, H. Late Precambrian Keweenawan asymmetric reversals. *Nature* **294,** 436–439 (1981).
2. Nevanlinna, H. & Pesonen, L. Late Precambrian Keweenawan asymmetric polarities as analyzed by axial offset dipole geomagnetic models. *J. Geophys. Res.* **88,** 645–658 (1983).
3. Van Schmus, W. R. & Hinze, W. J. The midcontinent rift system. *Annu. Rev. Earth Planet. Sci.* **13,** 345 (1985).
4. Halls, H. & Pesonen, L. Paleomagnetism of Keweenawan rocks. *Geol. Soc. Am. Mem.* **156,** 173–201 (1982).
5. Dubois, P. Paleomagnetism and correlation of Keweenawan rocks. *Bull. Geol. Surv. Can.* **71,** 1–75 (1962).
6. Robertson, W. & Fahrig, W. The great Logan Loop—the polar wandering path from Canadian shield rocks during the Neohelikian era. *Can. J. Earth Sci.* **8,** 1355–1372 (1971).
7. Weil, A., Van der Voo, R., Mac Niocaill, C. & Meert, J. The Proterozoic supercontinent Rodinia: Paleomagnetically derived reconstructions for 1100 to 800 Ma. *Earth Planet. Sci. Lett.* **154,** 13–24 (1998).
8. Buchan, K. *et al.* Rodinia: The evidence from integrated palaeomagnetism and U–Pb geochronology. *Precambr. Res.* **110,** 9–32 (2001).
9. Piper, J. The Neoproterozoic supercontinent Palaeopangea. *Gondwana Res.* **12,** 202–227 (2007).
10. Kent, D. & Smethurst, M. Shallow bias of paleomagnetic inclinations in the Paleozoic and Precambrian. *Earth Planet. Sci. Lett.* **160,** 391–402 (1998).
11. Evans, D. Stratigraphic, geochronological, and paleomagnetic constraints upon the Neoproterozoic climatic paradox. *Am. J. Sci.* **300,** 347–433 (2000).
12. Maloof, A. *et al.* Combined paleomagnetic, isotopic and stratigraphic evidence for true polar wander from the Neoproterozoic Akademikerbreen Group, Svalbard, Norway. *GSA Bull.* **118,** 1099–1124 (2006).
13. Palmer, H. Paleomagnetism and correlation of some Middle Keweenawan rocks, Lake Superior. *Can. J. Earth Sci.* **7,** 1410–1436 (1970).
14. Robertson, W. Pole positions from the Mamainse Point Lavas and their bearing on a Keweenawan pole path. *Can. J. Earth Sci.* **10,** 1541–1555 (1973).
15. Hanson, R. *et al.* Coeval large-scale magmatism in the Kalahari and Laurentian Cratons during Rodinia assembly. *Science* **304,** 1126–1129 (2004).
16. Shirey, S., Klewin, K., Berg, J. & Carlson, R. Temporal changes in the sources of flood basalts: Isotopic and trace element evidence for the 1100 Ma old Keweenawan Mamainse Point Formation, Ontario, Canada. *Geochim. Cosmochim. Acta* **58,** 4475–4490 (1994).
17. Symons, D. *et al.* Synopsis of paleomagnetic studies in the Kapuskasing structural zone. *Can. J. Earth Sci.* **31,** 1206–1217 (1994).
18. Lewchuk, M. & Symons, D. Paleomagnetism of the Late Precambrian Coldwell Complex. *Tectonophysics* **184,** 73–86 (1990).
19. McFadden, P. & McElhinny, M. Classification of the reversal test in palaeomagnetism. *Geophys. J. Int.* **103,** 725–729 (1990).
20. McElhinny, M., McFadden, P. & Merrill, R. The time-averaged paleomagnetic field 0–5 Ma. *J. Geophys. Res.* **101,** 25007–25027 (1996).
21. Besse, J. & Courtillot, V. Apparent and true polar wander and the geometry of the geomagnetic field over the last 200 Myr. *J. Geophys. Res.* **107,** 2300 (2002).
22. Evans, D. Proterozoic low orbital obliquity and axial-dipolar geomagnetic field from evaporite palaeolatitudes. *Nature* **444,** 51–55 (2006).
23. Tauxe, L. & Kent, D. in *Timescales of the Paleomagnetic Field* Vol. 145 *of Geophysical Monograph* (eds Channell, J., Kent, D., Lowrie, W. & Meert, J.) 101–116 (American Geophysical Union, 2004).
24. Elston, D. P., Enkin, R. J., Baker, J. & Kisilevsky, D. K. Tightening the belt: Paleomagnetic-stratigraphic constraints on deposition, correlation, and deformation of the middle Proterozoic (ca. 1.4 Ga) Belt-Purcell supergroup, United States and Canada. *GSA Bull.* **114,** 619–638 (2002).
25. Gallet, Y., Pavlov, V., Semikhatov, M. & Petrov, P. Late Mesoproterozoic magnetostratigraphic results from Siberia: Paleogeographic implications and magnetic field behavior. *J. Geophys. Res.* **105,** 16481–16499 (2000).
26. Davis, D. & Green, J. Geochronology of the North American Midcontinent rift in western Lake Superior and implications for its geodynamic evolution. *Can. J. Earth Sci.* **34,** 476–488 (1997).
27. Conrad, C. & Hager, B. Mantle convection with strong subduction zones. *Geophys. J. Int.* **144,** 271–288 (2001).
28. Evans, D. True polar wander and supercontinents. *Tectonophysics* **362,** 303–320 (2003).
29. Kirschvink, J. The least-squares line and plane and the analysis of paleomagnetic data. *Geophys. J. R. Astron. Soc.* **62,** 699–718 (1980).
30. Giblin, P. E. *Preliminary Geological Maps* 553–555 (Ontario Department of Mines, 1969).

Acknowledgements

We thank D. Jones, C. Rose and N. Eichelberger for field assistance; C. Bayne of Bay Niche Conservancy for land access; D. Kent and M. Jackson for assistance with hysteresis experiments; J. Kasbohm for help drafting the geological map; J. Kirschvink for support of pilot analyses at the Caltech Paleomagnetics Laboratory; and R. Mitchell and T. Kilian for support in the Yale palaeomagnetism facility, which was funded by NSF and the David and Lucile Packard Foundation. This work has benefited from discussions with D. Davis, J. Feinberg, H. Halls, D. Kent, B. Kopp, T. Raub and L. Tauxe. D. Bice encouraged N.L.S.-H. to begin study of Keweenawan volcanics when N.L.S.-H. was an undergraduate at Carleton College. This work was financially supported through a Sigma Xi Grant-In-Aid awarded to N.L.S.-H., A.C.M.'s Agouron Post-doctoral fellowship and Princeton University. B.P.W. acknowledges support from the NSF Geophysics Program.

Author contributions

Fieldwork was conducted by N.L.S.-H. (2 field seasons), A.C.M. (2 field seasons) and B.P.W. (1 field season) following initial project planning by A.C.M. and subsequent project planning by A.C.M. and N.L.S.-H. Samples were analysed by N.L.S.-H. in the laboratories of D.A.D.E. and B.P.W. N.L.S.-H. analysed the data, wrote the manuscript and drafted Figs 2–3 with input from A.C.M., B.P.W. and D.A.D.E. Figure 1 was drafted by A.C.M. and N.L.S.-H.

Additional information

Supplementary information accompanies this paper on www.nature.com/naturegeoscience. Reprints and permissions information is available online at http://npg.nature.com/reprintsandpermissions. Correspondence and requests for materials should be addressed to N.L.S.-H.

nature geoscience

SUPPLEMENTARY INFORMATION

DOI: 10.1038/NGEO622

Supplementary Information

S1 Additional data and methods

S1.1 Palaeomagnetic methods

A combination of 4 low-field (2.5, 5, 7.5 and 10 mT) 3-axis alternating field (AF) and 17-20 thermal demagnetization steps were applied to the specimens in order to construct detailed Zijderveld plots for principal component analysis[1]. The low-field AF steps had minimial effect on remanence or direction and were only applied to some of the specimens. A subset of specimens was treated with a low-temperature (77 K) thermal cycle in zero field where passage through the Verwey (110-120 K) transition preferentially demagnetizes multi-domain magnetite, leaving remanence carried by single-domain magnetite mostly intact[2,3].

High-temperature thermal demagnetization was performed in a furnace with 99% nitrogen atmosphere in order to limit oxidative mineralogical changes during demagnetization. Thermal demagnetization steps were initially as coarse as 100°C but fined to 5-15 °C through the characteristic unblocking temperatures of magnetite and hematite. Typical thermal demagnetization steps were: 100°C, 175°C, 250°C, 325°C, 400°C, 450°C, 500°C, 525°C, 550°C, 565°C, 575°C, 590°C, 620°C, 640°C, 640°C, 650°C, 660°C, 670°C, 670°C, 675°C.

A note for future workers: our usual practice in the field was to knock out the rocks from which the cores were drilled when we were working on sections along the shore. This was not always possible, but when it was, we employed this protocol in order to minimize the visible mark that we were making along this pristine stretch of the Lake Superior shoreline. When we encountered core holes drilled by previous workers (likely Palmer and Robertson) we left the core holes alone and intact. When we sampled along road cuts, however, we made no attempt to knock out our core holes and at this time they can readily be located. Also worth noting is the fact that the low lake levels during our 2007 field season fortuitously exposed a number of flows within the upper reversed zone that are commonly submerged.

S1.2 Palaeomagnetic data

Representative vector component diagrams are shown in Figures S1 and S2. Fisher means calculated for each flow are shown in Table S1. Summary results for the two conglomerate tests (MP45 and MP101) are shown in Figure S3. Summary palaeopoles that are plotted in Figure 3 of the main text are shown in Table S2. The poles plotted in Figure 3 were calculated as the Fisher mean of flow virtual geomagnetic poles (VGP) from the intervals shown in Figure 2 of the main text using the software of Cogne (2003)[4]. The poles that result from the alternate method of calculating a pole from the Fisher mean of the palaeomagnetic directions are also presented in Table S2. We chose to display the mean calculated from the VGPs in Figure 3 as the largest source of dispersion in the data is likely that from secular variation, which should have a circular distribution in accordance with the GAD hypothesis.

Previous workers have suggested that the difference in direction between reversed and normal directions could result from incomplete removal of viscous present local field overprints[5]. Detailed demagnetization routines reveal that the magnetizations of the Mamainse Point basalts do not contain any appreciable present local field overprint, and there is no reason to suspect that such overprinting is skewing least-square fits to components that unblock at high temperatures. A few flows have overprints of the subsequent opposite polarity that are likely due to proximity to feeder dykes of subsequent flows or to the emplacement of felsic intrusive bodies (see example in Fig. S1). Because these overprints are readily recognized in detailed Zijderveld plots, however, their ChRM can still be identified.

DOI: 10.1038/NGEO622

A number of flows, particularly within the lower normal and upper reversed zone but in the upper normal as well, have an additional magnetization component that unblocks between 590-650°C that is of opposite polarity to the components that unblock between 500-575°C and between 650-675°C (see MP209-5.4 in Fig. S2). For flows without this component there is generally little movement in the vector component plots between 590-650°C. The components that unblock between 500-575°C and between 650-675°C can be confidently interpreted as being carried by magnetite and hematite, respectively. The magnetic phase that carries the 590-650°C component is currently unresolved. The component can be found in one flow and not in the flow that is immediately above or below it stratigraphically. This context suggests that the component is not a pervasive chemical overprint or a thermal overprint, but is instead related to the original mineralogy of the flow. One possibility is that it is a self-reversing titanohematite with a composition close to $Fe_{1.9}Ti_{0.1}O_3$ so that the Curie temperature is not very suppressed. Such a component was observed in the Bucks batholith above the Curie point of magnetite when the magnetization of the samples switched from normally magnetized to reversed and were throughly demagnetized by ~630°C[6]. More rock magnetic experiments will be necessary to determine the phase that holds this remanence.

S1.3 Palaeomagnetic conglomerate tests

Conglomerate tests were conducted on basalts clasts from both the basalt clast conglomerate (site MP45; Fig. S11) and the great conglomerate (site MP201; Fig. S11). For the MP45 conglomerate test (Fig. S3), the 17 fits through the haematite blocking temperatures have a resultant vector length (R) of 3.91, below the R_0 value of 6.65 for n=17. Thus, randomness cannot be rejected as $R<R_0$. 11 of the MP45 samples had a significant percentage of remanence lost through magnetite unblocking temperatures and the magnetite least squares fit have a resultant vector length (R) of 3.52, below the R_0 value of 5.35 for n=11. For the MP201 conglomerate test (Fig. S3), the R value for the 26 haematite fits is 2.01 below the R_0 of 8.23. The R value for the 23 magnetite fits is 2.28 below the R_0 of 7.24. As stated in the main text, these conglomerate test results further confirm that both the magnetite and haematite components observed in the flows were acquired prior to the erosion of the flows and the deposition of these conglomerates that were laid down within the larger stack of Keweenawan basalts.

A previous conglomerate test on the great conglomerate showed that at 80 mT of AF demagnetization magnetization directions passed a conglomerate test but that there was a lower coercivity component that was coincident in direction with the upper Mamainse Point normal flows[7]. However, the authors concluded that this secondary component was not biasing the characteristic remanent magnetization of the samples. We found no such secondary component at the MP101 site. This is not surprising, as it would be expected that remagnetizations associated with subsequent volcanism would be spatially limited and related to the locale's proximity to overlying flows or feeder dykes.

S1.4 Rock magnetic data

Magnetic hysteresis loops were measured with an alternating gradient force magnetometer (Figs. S4 and S5) and a vibrating sample magnetometer (Fig. S6). It is visually apparent in the hysteresis loops that samples with low squareness (a low M_r/M_s ratio which makes for a skinny loop) have a high removal of remanence through the unblocking temperatures of magnetite. Correspondingly, the samples with a high squareness value are samples where much of the magnetization is carried by components that unblock above 590°C. This relationship is further apparent in the cross-plot of "% remanence lost by 590°C" versus squareness (Fig. S7B). This relationship does not explain all the charecteristics of the hysteresis data as changes in distribution of the magnetite size fractions should also have an effect, but the amount of hematite in a

sample appears to be a major factor in determining its rock magnetic behaviour, which also explains the strong correlation between squareness and the bulk coercive field (B_c; Fig. S7b).

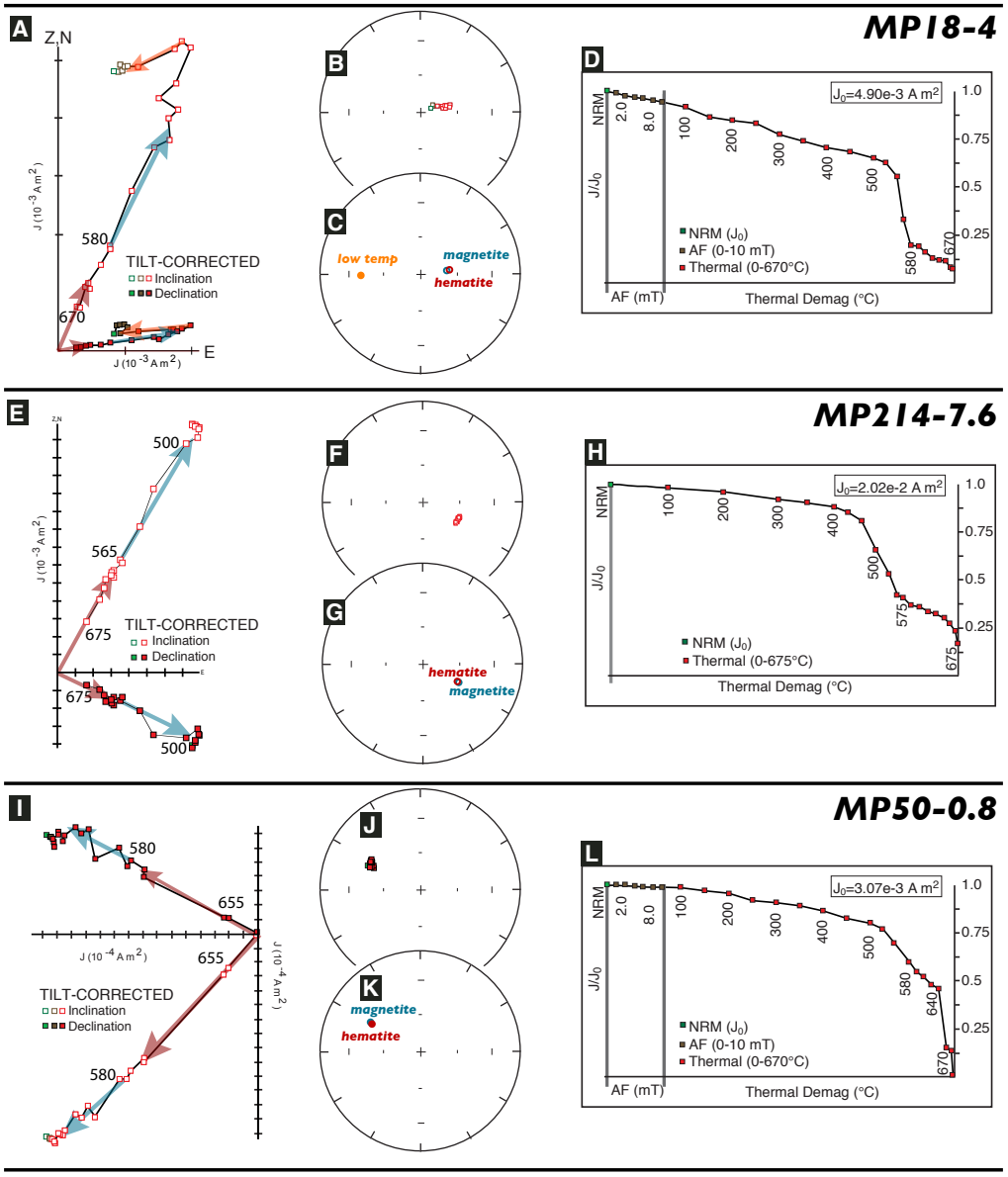

Figure S1: Representative vector component diagrams (Zijderveld, 1967) (A, E, and I), equal-area projections (B, F, and J), least-squares fits (C, G, and K), and magnetic intensity (J/J0) plots (D, H, and L) showing demagnetization behaviour for Maminse Point basalts. The magnetic intensity plots are normalized for demagnetization line length so that no subsequent value can be higher than the initial intensity. In the Zijderveld plots the primary, high-temperature component is separated into the hematite component, traced with a red arrow, and a magnetite component, traced with a blue arrow. MP18-4 has a low-temperature overprint, removed by 200°C, that is traced with an orange arrow. Least-squares fits of these components are summarized in an adjacent equal-area projection (C, G, and K). In all plots, green-filled shapes are natural remanent magnetization (NRM) directions, brown-filled shapes reflect alternating field (AF) demagnetization steps, and red-filled shapes reflect thermal demagnetization. In the Zijderveld plots (A, E, and I) closed-squares/open-squares represent declination/inclination, while in the equal-area nets (C, G, and K), colour-filled/colour-rimmed circles represent lower/upper-hemisphere directions. All data is presented in tilt-corrected coordinates

DOI: 10.1038/NGEO622

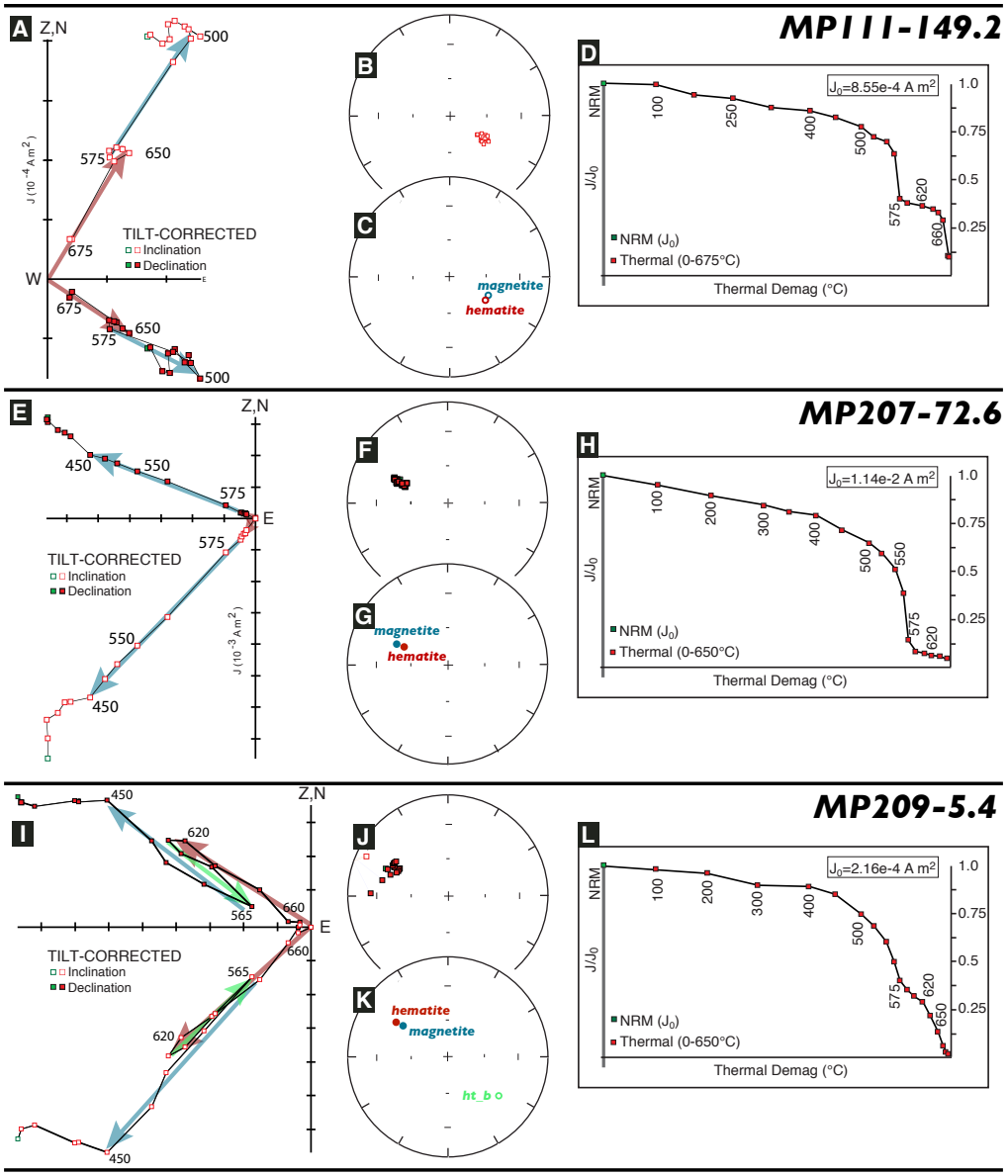

Figure S2: Representative vector component diagrams (Zijderveld, 1967) (A, E, and I), equal-area projections (B, F, and J), least-squares fits (C, G, and K), and magnetic intensity (J/J0) plots (D, H, and L) showing demagnetization behaviour for Maminse Point basalts. The magnetic intensity plots are normalized for demagnetization line length so that no subsequent value can be higher than the initial intensity. In the Zijderveld plots the primary, high-temperature component is separated into the hematite component, traced with a red arrow, and a magnetite component, traced with a blue arrow. MP209-5.4 has a component, unblocked between 565 and 605 °C and traced with a green arrow, whose direction is antiparallel to the other two components. Least-squares fits of these components are summarized in an adjacent equal-area projection (C, G, and K). In all plots, green-filled shapes are natural remanent magnetization (NRM) directions, brown-filled shapes reflect alternating field (AF) demagnetization steps, and red-filled shapes reflect thermal demagnetization. In the Zijderveld plots (A, E, and I) closed-squares/open-squares represent declination/inclination, while in the equal-area nets (C, G, and K), colour-filled/colour-rimmed circles represent lower/upper-hemisphere directions. All data is presented in tilt-corrected coordinates.

Table S1: Palaeomagnetic data for flows from the Mamainse Point succession

flow number	flow ID	section meter level	composite meter level	n	Geographic		Tilt-corrected		α_{95}	κ	fit used
					D_m	I_m	D_m	I_m			
1	MP101a	0.0 to 15.5	68	6	203.2	-50.3	131.6	-63.2	9.2	54	mag
2	MP101b	20.7 to 21.3	89	4	209.1	-46.8	141.5	-66.4	8.4	121	mag
3	MP101c	22.3 to 24.2	90	4	219.1	-53.5	122.6	-72.9	9.6	93	mag
4	MP101d	36.7 to 37.4	105	6	209.4	-53.1	125.8	-67.2	6.6	105	mag
5	MP101e	40.7 to 42.4	109	4	205.1	-54.7	122.0	-64.6	2.6	1205	hem
6	MP18	daisy stone	222	6	249.8	-62.9	78.6	-75.0	3.3	419	mag
7	MP105a	0.0 to 6.9	370	4	212.4	-51.8	120.3	-67.1	6.9	179	mag
8	MP105b	20.2 to 27.3	390	6	240	-47.5	94.7	-84.7	1.8	1343	mag/hem (4/2)
9	MP105c	27.3 to 29.6	397	4	231.7	-48.0	119.6	-80.1	4.7	384	hem
10	MP105e	32.5 to 35.1	402	6	244.4	-56.5	63.2	-76.5	5.8	134	mag/hem (4/2)
11	MP107a	0.0 to 3.8	584	6	231.9	-55.4	99.6	-70.9	6.5	109	mag
12	MP107b	3.8 to 10.2	587	5	233.9	-57.6	92.9	-69.9	2.7	814	mag/hem (3/2)
13	MP107c	11.3 to 14.6	595	6	226.9	-63.0	91.6	-63.5	5.8	135	hem
14	MP107d	14.6 to 20.0	598	5	235.5	-59.6	88	-68.7	8.6	80	mag
15	MP43a	0.0 to 2.8	1080	3	224	-72.4	105.8	-46.5	8.4	216	hem
16	MP43b	2.8 to 7.1	1083	4	238.4	-67.3	106.7	-53.5	8.9	108	hem
17	MP43c	16.7 to 25.4	1096	4	241.2	-59	115.9	-60.2	12.7	53	hem
18	MP43d	25.4 to 33.4	1105	3	235.6	-66.4	109.1	-53.4	8.7	203	hem
19	MP43f	33.4 to 43.6	1113	5	237.4	-77.7	104.5	-59.6	8.3	87	mag
20	MP121a	10.6 to 14.4	1182	4	267.7	-68.8	107.1	-70.6	6.8	182	hem
21	MP121b	23.3 to24.4	1194	4	267.8	-77.9	101.1	-61.9	4.5	422	hem
22	MP121c	27.6 to 31.3	1199	4	252	-75.5	110.3	-62.6	9.2	101	mag/hem (3/1)
23	MP121d	46.6 to 49.4	1205	4	262	-68.9	112.6	-69.8	2.4	1512	hem
24	MP214a	0.0 to 5.4	1290	3	175.2	-73.6	102.1	-53.9	5.4	513	mag
25	MP214b	6.6 to 8.8	1297	4	192.6	-76.5	96.7	-56.9	8.5	118	mag
26	MP214c	11.0 to 13.1	1301	4	167.1	-77.6	95	-53.3	16.4	32	mag/hem (1/3)
	MP45	conglomerate	1325	19	75.9	11.4	71.4	51	101.6	1	hem
27	MP214d	60.3 to 67.9	1351	5	10.6	71.8	286	58.3	5.2	218	mag
28	MP214e	73.4 to 79.1	1364	2	340.8	76	276.5	51	15.6	259	mag
29	MP214f	79.1 to 90.0	1370	5	314.2	78.2	269.2	47	6.7	131	mag
30	MP46a	0.0 to 7.0	1384	8	324.6	72.1	283.5	39.4	5.5	103	mag
31	MP46b	7.0 to 8.0	1387	3	316.6	70.2	282.8	36.3	16.2	59	hem
	MP48	sst in con	1744	6	359.8	64.6	305.2	45.1	3	413	hem
32	MP49a	0.0 to 1.7	1776	3	345.5	57.4	310.9	34.8	11.7	113	mag
33	MP49b	1.7 to 5.6	1778	5	344	60.4	307.7	36.2	3.1	599	mag
	MP50a	sst	1763	3	354.7	64.5	299.8	50.2	8.2	151	hem
34	MP50b	0.9 to 12.1	1764	4	357.8	64.2	301.3	51.2	6.4	89	mag
35	MP50c	12.1 to 15.1	1775	5	6.4	74.3	286.1	56.9	8.3	86	mag
36	MP111a	0.0 to 5.3	1782	6	30	60.3	321.4	58.4	11.6	45	hem
37	MP111b	5.3 to 18.2	1788	6	16.8	70.5	301.3	54.8	11.9	33	mag/hem (2/4)
38	MP111c	18.2 to 23.4	1801	4	45.6	69.8	300.8	64.5	6.4	145	mag/hem (1/3)
39	MP111e†	37.6 to 43.1	1820	6	350.2	36.7	328.7	24.4	3.6	341.4	hem
40	MP111f†	50.4 to 69.2	1833	6	350.3	41	325.5	27.6	23.1	17	mag/hem (3/1)
41	MP111g†	75.5 to 82.8	1858	5	336.3	40.9	316.7	20.8	13	36	mag/hem (4/1)
42	MP53	0.0 to 6.6	1865	9	146.3	-72.2	106.7	-39	3.4	226	mag
43	MP54	0.0 to 4.0	1872	4	152.6	-74.8	105.7	-42.1	7.8	140	mag
44	MP111h	128.2 to 130.7	1910	5	136	-68.3	112.7	-33.9	7.8	97	mag/hem (2/3)
45	MP111i	130.7 to 141.9	1913	6	164.7	-77.1	113.3	-45.9	3.8	416	hem
46	MP111j	141.9 to 145.5	1924	5	166	-74.3	116.9	-44.5	4.7	268	hem
47	MP111k	145.5 to 147.1	1928	6	183	-67	129.8	-45.4	4.9	250	hem

DOI: 10.1038/NGEO622

Table S1: Palaeomagnetic data for flows from the Mamainse Point succession (continued)

flow number	flow ID	section meter level	composite meter level	n	Geographic		Tilt-corrected		α_{95}	κ	fit used
					D_m	I_m	D_m	I_m			
48	MP111l	147.1 to 150	1930	3	182.4	-70.9	124.7	-47.1	5.4	155	mag/hem (3/3)
49	MP111m	154.2 to 160.6	2085	6	166.1	-68.3	123.3	-40.9	8.7	113	mag
50	MP111b-n	273.8 to 282.7	2056	5	6.3	-84.4	86.9	-51.6	13.6	32	mag/hem (3/2)
51	MP111b-o	302.2 to 310.0	2085	3	184.7	-80.9	100.5	-50.9	6	235	mag
	MP201	conglomerate	2106	23	248.1	32.3	250.8	-1.8	106.3	1	mag
52	MP207a	0.0 to 20.4	2413	5	320.1	68.2	297.4	36.7	4.2	336	mag
53	MP207b	20.4 to 40.8	2426	5	322.6	68.9	297.9	37.8	4.9	248	mag
54	MP207c	42.3 to 43.5	2448	6	335.5	74	298.5	44.2	3.1	478	mag
55	MP207d	45.0 to 53.3	2451	6	317.9	72.7	293.8	40.4	5.7	137	mag
56	MP207e	53.7 to 62.6	2459	7	334.2	75.6	296.6	45.2	4.9	155	mag
57	MP207f	62.6 to 71.5	2468	6	310.8	75.3	290.9	41.9	9.2	54	mag
58	MP207g	71.5 to 85.5	2477	5	306.2	74.1	289.1	40.3	3.1	612	mag
59	MP209a	1.2 to 7.3	2482	5	325.9	70.6	293.7	45.3	6.8	99	mag
60	MP209b	7.3 to 20.3	2488	6	348	72.5	299	51.5	5.5	148	mag
61	MP209c	20.3 to 33.6	2501	7	315.5	70.2	289.9	43	6.1	120	mag
62	MP209d	33.6 to 42.2	2514	7	321.1	61.5	298.1	36.6	6.2	97	mag
63	MP209e	42.2 to 51.1	2523	6	333.9	63	303.5	41.1	5	179	mag
64	MP209f	51.1 to 65.5	2532	5	303.6	63.3	288.1	34.8	3.4	378	mag
65	MP211a	34.9 to 38.1	2610	3	313.9	53.5	296.6	27.4	5.8	451	mag
66	MP211b	39.2 to 46.6	2615	4	308.6	64.3	290.7	36.4	4.9	351	mag
67	MP211c	48.0 to 56.1	2623	4	317.1	58.8	297.9	33.1	5.2	311	mag
68	MP211d	69.9 to 87.2	2645	5	305.9	55.8	292.8	27.9	4.2	339	mag
69	MP212a	0.0 to 10.2	3045	4	326.4	61.9	298.5	42.6	6.1	232	mag
70	MP212b	10.2 to 15.5	3055	6	323.5	60.2	298.2	40.3	5.8	135	mag
71	MP212c	15.5 to 22.2	3060	5	322.7	63.9	295.1	43.2	6.8	128	mag
72	MP212d	22.2 to 30.8	3067	5	318.3	59.7	295.7	38.6	6.4	142	mag

Notes: n, D_m, I_m, α_{95}, κ - number of samples analyzed per flow, mean declination, mean inclination, 95% radius of confidence for palaeomagnetic direction and Fisher precision parameter. The "mag" fits are weighted fits typically through the 500°C, 525°C, 550°C, 565 °C and 575°C thermal demagnetization steps calculated using the routines of[8]. "Hem" fits are weighted least-squares fits through the uppermost thermal steps typically 640°C, 650°C, 660°C, 670 °C and 675°C. Means calculated from both "mag" and "hem" directions are denoted "mag/hem" with the number of each type used denoted in parentheses "(# of mag/ # of hem)". Flows with a † are at the top of the lower normal chron and have an anomalous declination grouping. They may be transitional directions or associated with an excursion and were not included in plots or statistical analysis. Flows with α_{95} 12 were not included in the equal-area plot of Fig. 2d for the sake of clarity but were included in statistical analyses.

Table S2: Palaeomagnetic poles calculated from Mamainse Point data.

Fisher mean of direction						"Mean of directions" pole				"Mean of VGP" pole		
pole	D	I	α_{95}	κ	n	λ_p	ϕ_p	dp	dm	λ_p	ϕ_p	A_{95}
all reversed	289.2	60.0	4.3	32.0	36	40.5	205.6	4.9	6.5	39.9	207.4	5.4
all normal	295.3	43.0	3	70.6	32	35.0	185.6	2.7	4.3	33.2	186.5	2.8
lower Reversed 1	289.5	72.0	4.7	71.5	14	47.6	225.7	7.3	8.3	47.5	226.7	8.0
lower Reversed 2	285.1	58.6	4.2	109.0	12	37.0	206.1	4.6	6.2	37.5	206.7	5.1
lower Normal	295.2	49.8	8.3	31.0	11	38.5	191.0	7.4	11.1	38.0	190.8	9.7
upper Reversed	292.5	44.7	6.2	62.3	11	33.9	188.8	4.9	7.8	34.7	189.2	8.0
upper Normal	295.3	39.5	2.7	149.9	21	33.2	183.2	1.9	3.2	33.8	192.0	2.9

Notes: Reversed directions and poles are reversed so that all values are in "normal" coordinates. These poles are calculated from the intervals shown in Fig. 2 of the main text. The "Mean of directions pole" is the pole found when the Fisher mean calculated for directions is transformed into a palaeomagnetic pole. The "Mean of VGP pole" is the Fisher mean of the flow (site) VGPs

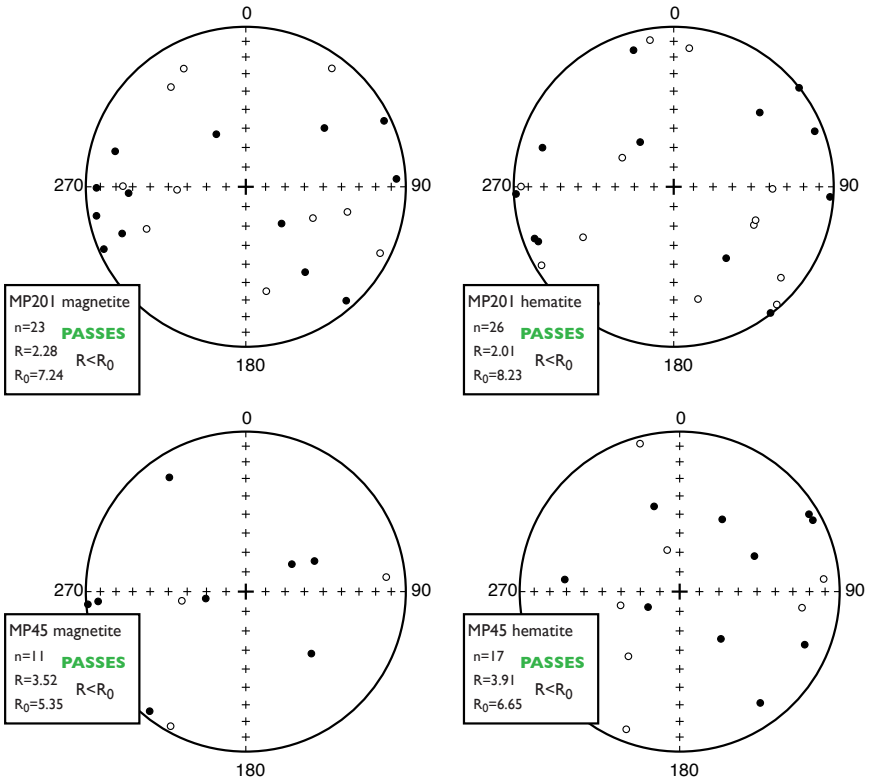

Figure S3: ChRM directions for the conglomerate tests in the basalt clast conglomerate (MP45) and the great conglomerate (MP201). All tests demonstrate that the directions are consistent with being selected from a random population as randomness can not be rejected at the 95% confidence level. This result shows that both the magnetite and hematite components observed in the flows were acquired prior to the erosion of the flows and the deposition on the conglomerates that were laid down within the larger stack of Keweenawan basalts.

DOI: 10.1038/NGEO622

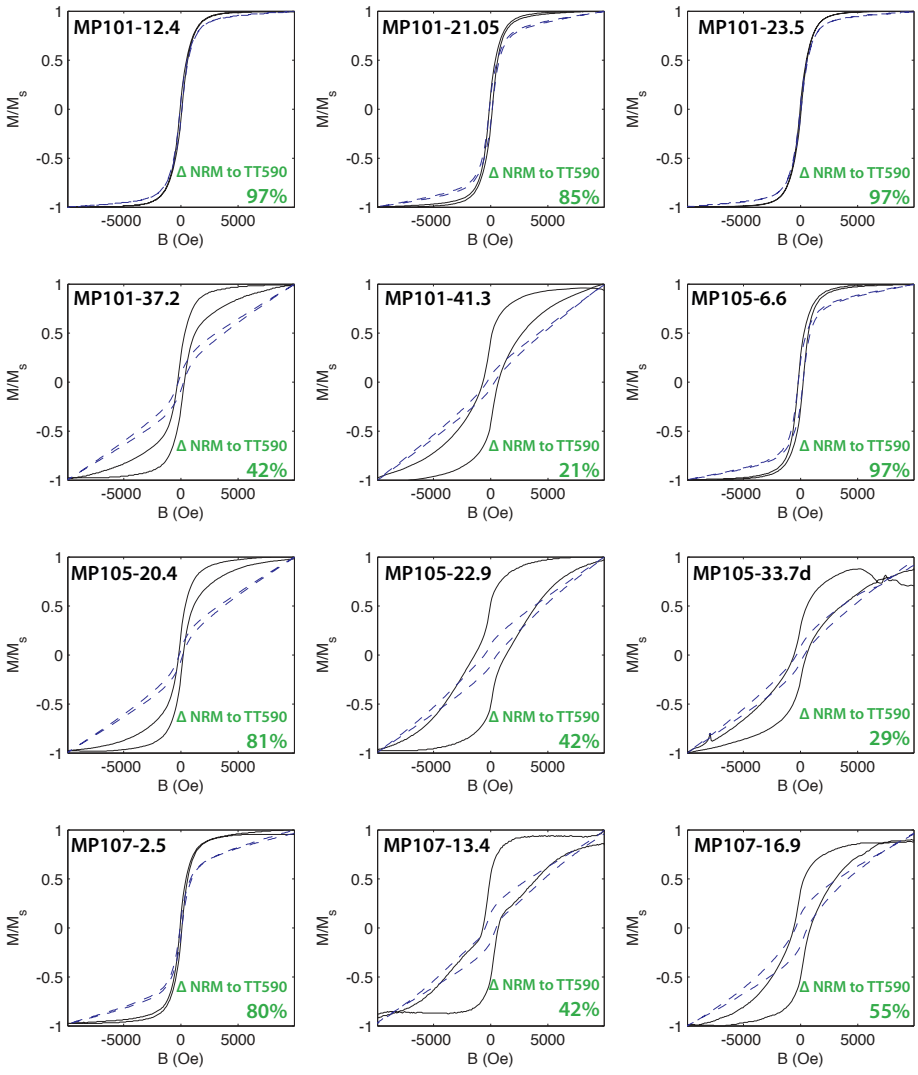

Figure S4: Hysteresis loops for basalt samples from the MP101, MP105 and MP107 sections. The blue dotted line is the original data (normalized to the highest value of M) while the black solid line has been slope corrected to remove the paramagnetic component. The magnetization shown on the y-axis normalized to the saturation magnetization (M_s). The percentage shown in the lower right of each plot is the percentage of the natural remanent magnetization that was removed by the 590°C thermal demagnetization step.

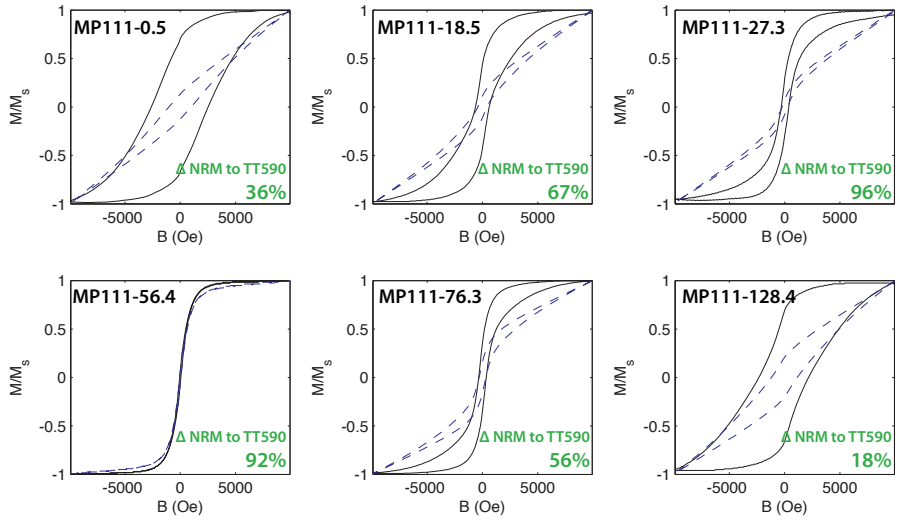

Figure S5: Hysteresis loops for basalt samples from the MP111 section. The blue dotted line is the original data (normalized to the highest value of M) while the black solid line has been slope corrected to remove the paramagnetic component. The magnetization shown on the y-axis normalized to the saturation magnetization (M_s). The percentage shown in the lower right of each plot is the percentage of the natural remanent magnetization that was removed by the 590°C thermal demagnetization step.

DOI: 10.1038/NGEO622

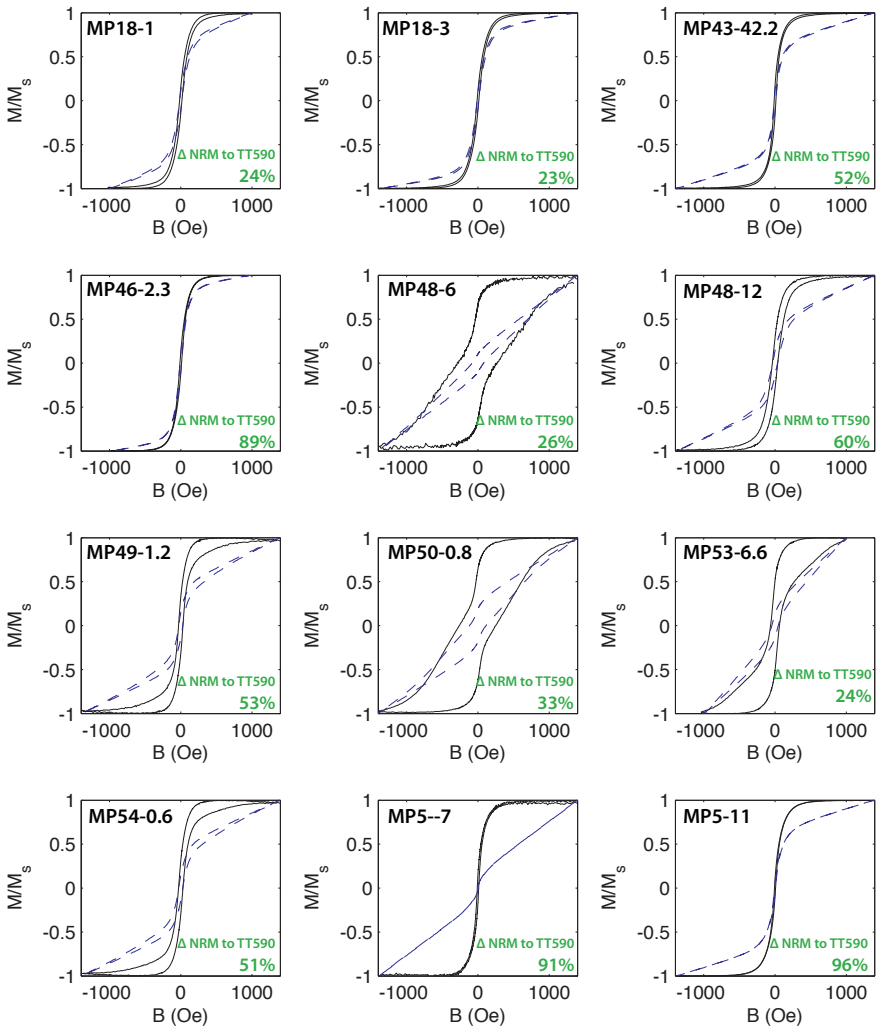

Figure S6: Hysteresis loops for basalt samples from the MP18, MP43, MP46, MP48, MP49, MP50, MP53, and MP54 section. The blue dotted line is the original data (normalized to the highest value of M) while the black solid line has been slope corrected to remove the paramagnetic component. The magnetization shown on the y-axis normalized to the saturation magnetization (M_s). The percentage shown in the lower right of each plot is the percentage of the natural remanent magnetization that was removed by the 590°C thermal demagnetization step. The sample MP5-11 is from a dyke north of the principal study area and is included for comparison to the flows.

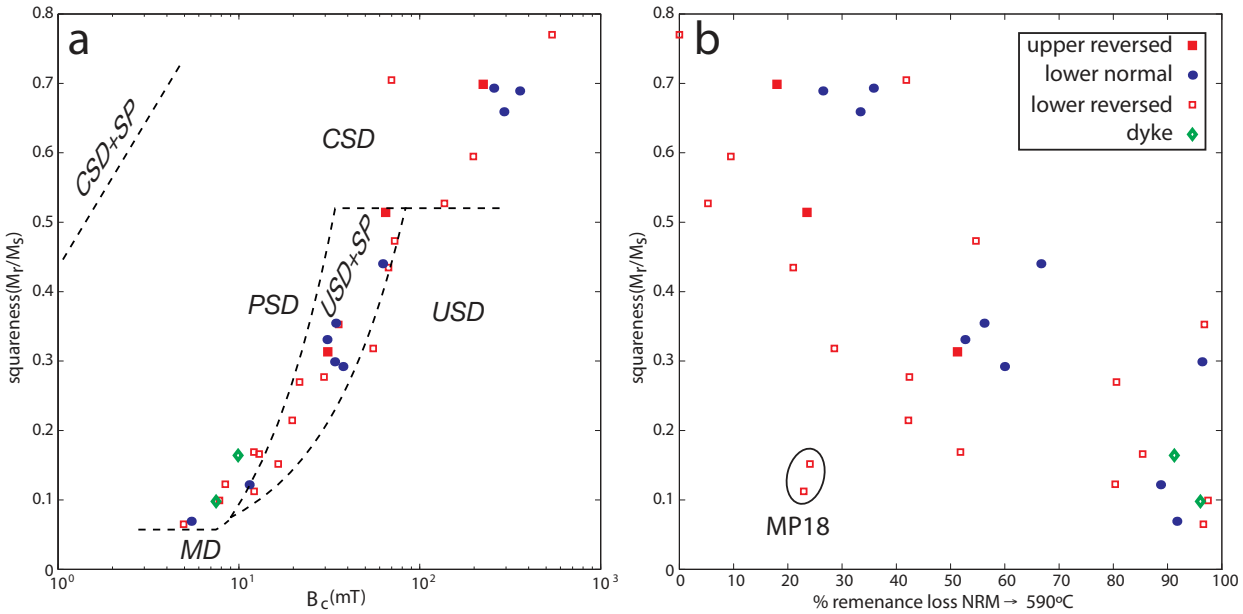

Figure S7: A) Summary plot of squareness (M_r/M_s) versus coercive field (B_c) for Mamainse Point Samples. The dashed black lines delineate the approximate boundaries for magnetite size fractions[9] (CSD is cubic single domain, USD is uniaxial single domain, PSD is pseudo single domain, SP is superparamagnetic, MD is multidomain). These boundaries are included as reference but given that most of the samples are a mix between hematite and magnetite components they can not be taken literally. Note the strong positive relationship between squareness and coercive force. Due to the higher coercivity of hematite than magnetite, this trend points to a relationship between the amount of hematite and squareness. B) Summary plot of squareness (M_r/M_s) versus % original remanence demagnetized by 590°C. % original remanence demagnetized by 590°C can be taken as a rough estimate of the percent of magnetite relative to hematite in each sample. Generally when the sample is more thoroughly demagnetized by 590°C the squareness of the hysteresis curve is lower. The two samples that are significantly off of this trend have been labeled "MP18" and are from the distinctive "daisy stone" flow which contains large plagioclase phenocrysts in radiating clusters (Fig. S12).

DOI: 10.1038/NGEO622

S1.5 Conglomerate clast counts

Previous palaeomagnetic studies at Mamainse Point have argued for a major duplicating fault to explain the multiple reversals as they were working within the paradigm that there was a single reversal in the history of the rift[5,10]. Palmer (1970) wished to correlate the lower "basalt clast conglomerate" with the stratigraphically higher "great conglomerate," but these conglomerates are of strikingly different composition. While the lower conglomerate consists entirely of clasts of locally derived basalt, the upper "great" conglomerate transitions from being ladened primarily with basalt clasts at its base to containing abundant basement-derived metamorphic clasts upwards in the succession. Five clast counts of ~50 clasts each were conducted through the great conglomerate to document this increase in metamorphic clasts up-section (Fig. S8). The fault repetition hypothesis can be dismissed on sedimentological ([11], this study), structural ([11,12], this study), geochemical[13,14] and palaeomagnetic grounds (this study). The change in provenance that caused the increase in basement-derived metamorphic clasts also points towards an extended timescale for the deposition of the conglomerate, though this timescale is difficult to quantify.

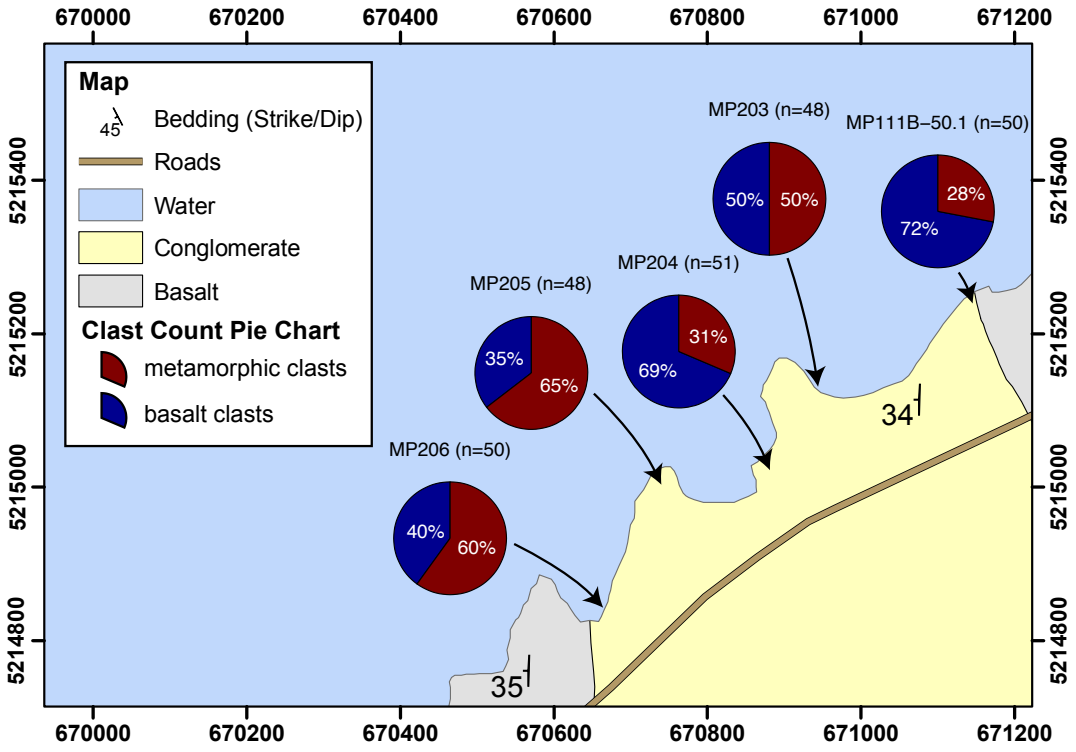

Figure S8: Clast composition through the "great conglomerate." X- and Y- axis labels are UTM (WGS84) coordinates in meters for zone 16N. Note that the percentage of clasts derived from the Superior Province metamorphics increases upwards (to the west) through the unit.

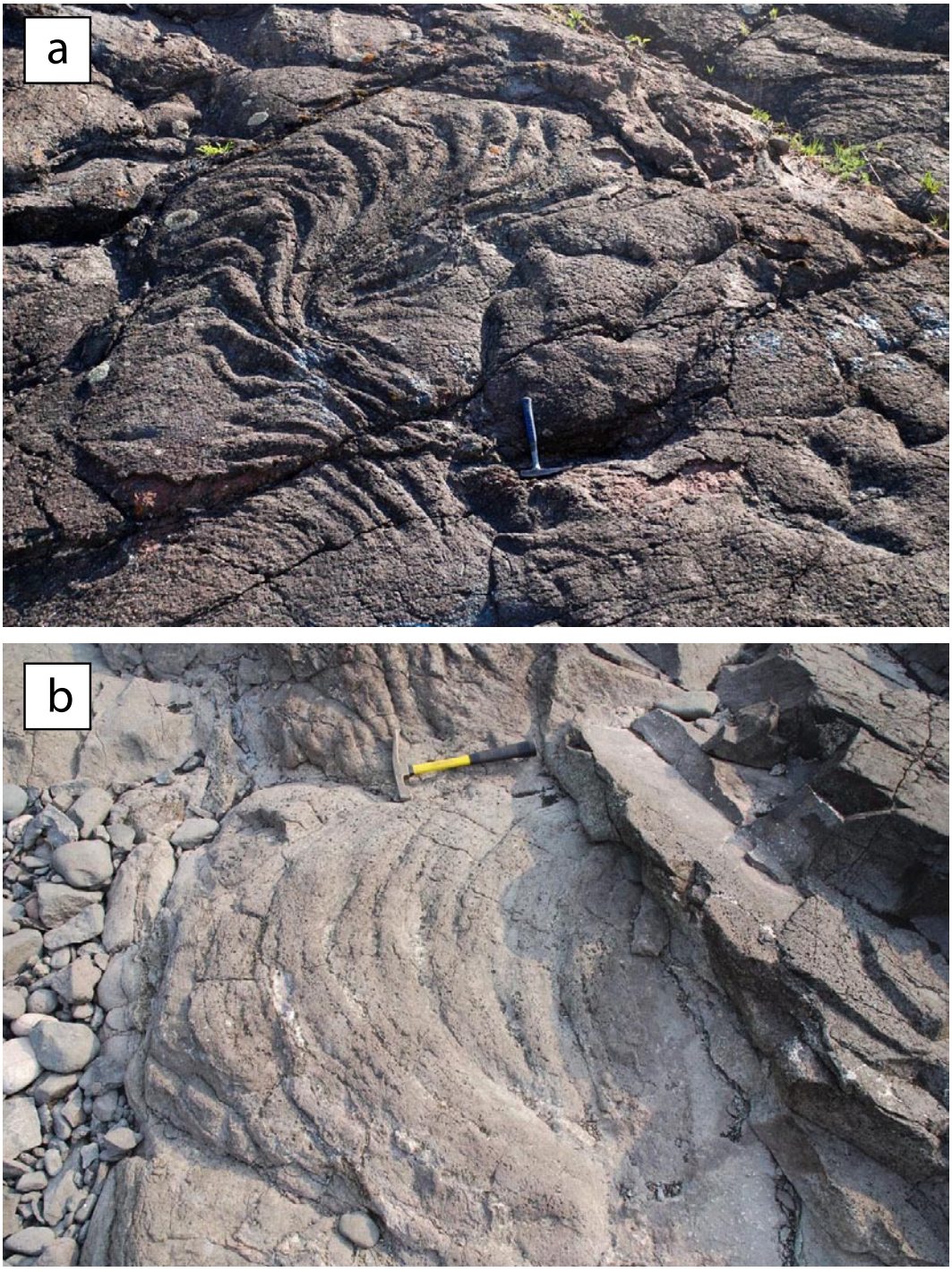

Figure S9: Pahoehoe flowbanding at the top of flows in the Mamainse Point succession. The upper photo (a) is from a road-cut in the lower reversed zone while the lower photo (b) is from a section along the shore in the upper normal zone. Hammers are $\sim$ 35 cm long.

DOI: 10.1038/NGEO622

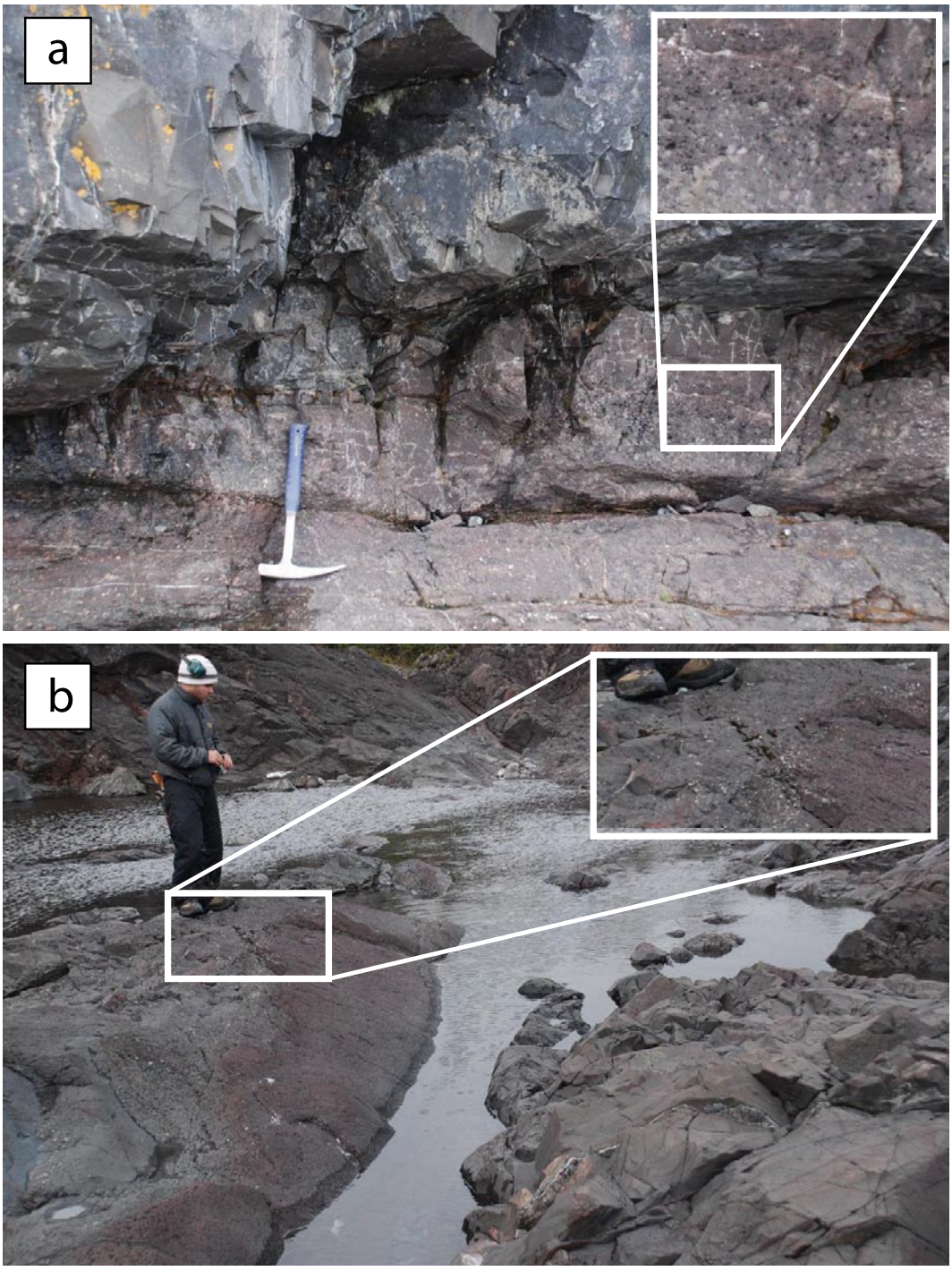

Figure S10: Typical flow tops in the Mamainse Point succession from the MP207 section that are highly vesiculated, slightly ferruginized and overlain by massive non-vesicular basalt of the next flow. The hammer in (a) is $\sim$ 35 cm long and the handle points towards stratigraphic up with the flow contact right above the end of the handle. Stratigraphic up is towards the right in (b) with some water at the actual contact between the highly vesiculated basalt of the lower flow and the massive basalt of the upper flow. Insets show enlarged views of highly vesiculated basalt at the tops of the flows.

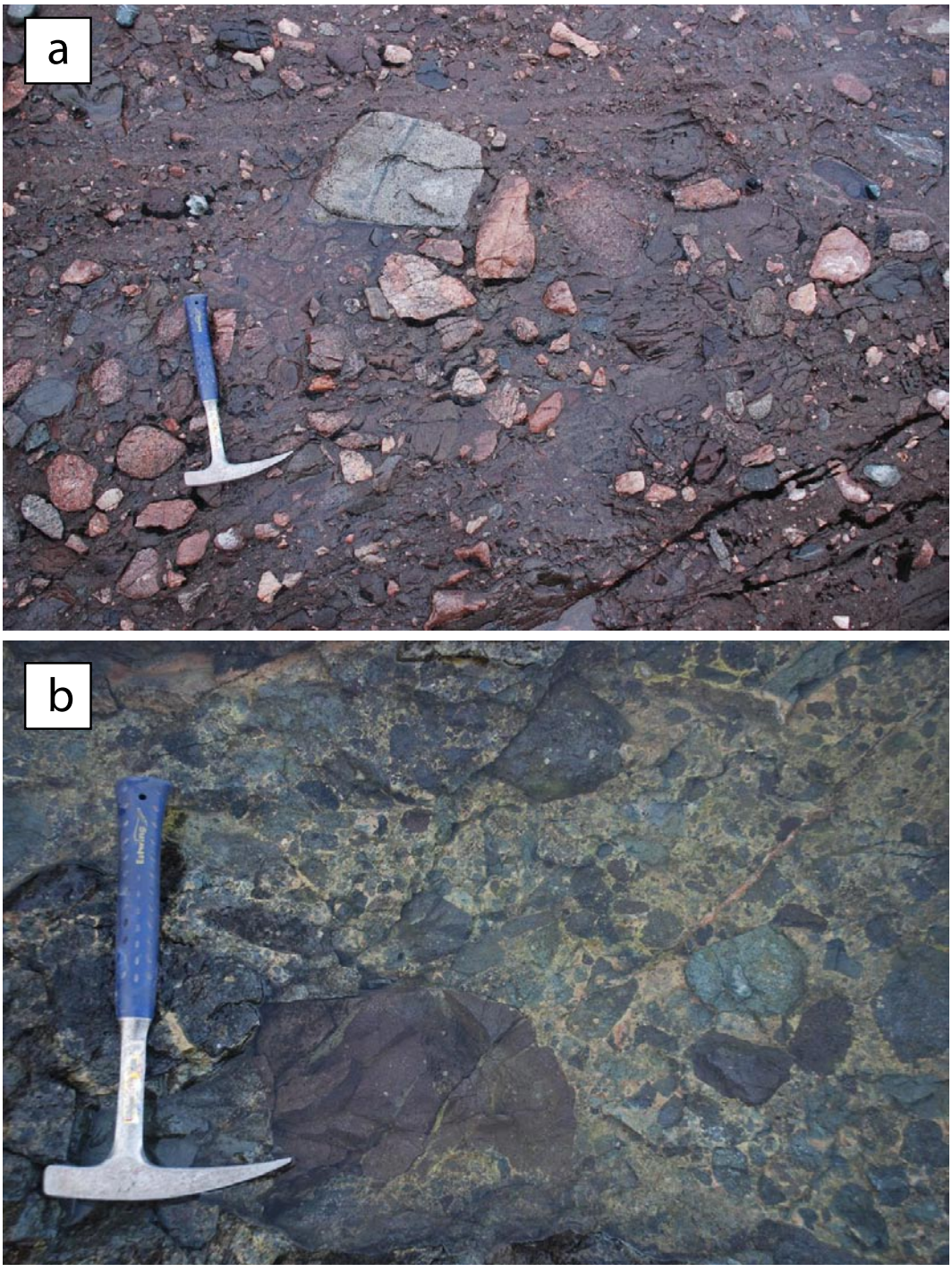

Figure S11: The polymict "great conglomerate" and the monomict "basalt clast Conglomerate." The photo of the great conglomerate (a) is from stratigraphically high within that unit where 60% of the clasts are composed of Superior Province metamorphic clasts. The clasts of the basalt clast conglomerate (b) are all basalt like most conglomerates that are interbedded with the flows. The hammer is $\sim$ 35 cm long.

DOI: 10.1038/NGEO622

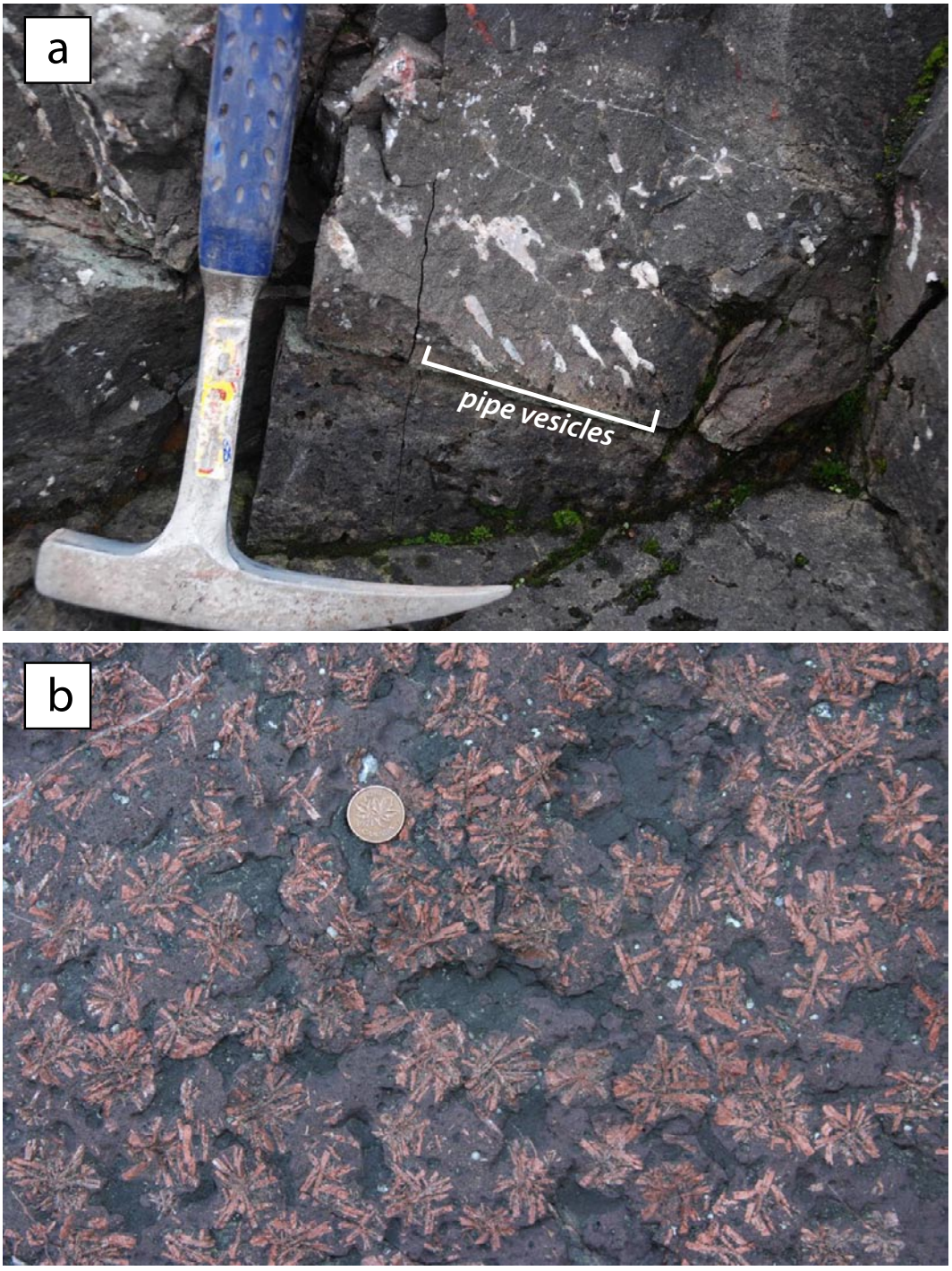

Figure S12: a) Elongate "pipe" vesicules at the base of a flow. The hammer head is $\sim$ 15 cm long. b) The "daisy" stone flow with its characteristic clusters of radiating plagioclase laths (site MP18).

S2 Palaeomagnetic data from other studies

S2.1 Prior palaeomagnetic studies at Mamainse Point

The palaeomagnetism of basalt flows at Mamainse Point has been studied before by Dubois (1962)[15], Palmer (1970)[5] and Robertson (1973)[10]. The study of Dubois[15] revealed reversed directions in equivalents to the lower Mamainse Point succession at nearby Alona Bay and normal directions high in the Mamainse Pointsuccession. Palmer[5] and Robertson[10] sampled at sufficient resolution to identify the 3 reversals in the succession. However, both authors favored the hypothesis that these multiple reversals were in fact a single reversal that had been fault-repeated as they were influenced by the conventional thinking at the time that there was a single geomagnetic reversal during the history of the rift. As a result of this interpretation, they did not evaluate the change in direction through the stratigraphy. As Palmer[5] wrote: "Although there is as yet no geological evidence to support the fault hypothesis, the magnetic evidence favoring repetition by faulting is tentatively accepted, and all normal directions and all reversed directions have been combined to yield a single normal mean direction and a single reverse mean direction." However, as Halls and Pesonen (1982)[16] pointed out, the upper reversed division had significantly lower inclination than the lower reversed division in both the studies of Palmer[5] and Robertson[10] (Table S3). Ernst (1992)[17] argued that the upper reversed direction of Robertson (1973)[10] was statistically indistinguishable from both the normal chrons; but, as Schmidt and Williams (2003)[18] asserted, since the upper reversed directions comes from only two flows no comparison test can be made that is statistically valid. The inability to draw firm conclusions about the changes in direction (or lack thereof) through the succession stems from the low resolution of the previous studies (as pointed out by[16–18]). Another factor that complicates the analysis of the previous data that has previously been developed at Mamainse Point is that the data reported were the directions after some chosen AF demagnetization step (100-200 mT), rather than least-squares fit to vector endpoints of progressive demagnetization as is the typical practice for modern palaeomagnetic studies[1]. While in general our results match those from previous studies quite well, we did not observe reversals to occur within the flows below the great conglomerate or the basalt clast conglomerate as was reported by Palmer[5]. The flows up to the conglomerates retain reversed polarity indicating that the reversals occurred during the deposition of the conglomerates.

An unpublished U-Pb zircon age from within the Mamainse Point succession (reported in an abstract from the Annual Meeting of the Institute on Lake Superior Geology[19]) has been discussed in peer-reviewed literature[20,21]. As reported in the abstract, the age was obtained from a felsic unit near the top of the lower reversed zone and is 1096.2 $\pm$1.9 Ma. The interpretation in the abstract was that this felsic body was extrusive and given that the age is younger than some normally magnetized flows there must have been at least 5 asymmetric reversals during Keweenawan volcanism. The location of the sampled unit[22] corresponds to a unit that has previously been mapped as a felsic intrusion (the first felsic intrusion beneath the basalt clast conglomerate in Fig. 2;[12]) and the date remains unpublished because it has proven difficult to establish that the unit is eruptive[20]. Although the quasi-bedding-parallel orientation of felsic intrusive bodies can complicate intrusive versus extrusive interpretations, we note the abundance of felsic intrusions in the area that more clearly cut across bedding that are particularly prevalent in the upper normal zone (e.g. the felsic intrusion at UTM: 522910 587197) and, like Giblin, we favor an intrusive interpretation for the dated unit.

S2.2 The fault hypothesis

When Palmer (1970)[5] discovered the multiple reversals in the sequence of basalts at Mamainse Point, this single reversal paradigm led him to propose the presence of a sequence-repeating fault, despite the fact that, in his words, there is "no geological evidence favoring that fault hypothesis." The fault repetition

DOI: 10.1038/NGEO622

Table S3: Palaeomagnetic data from other studies of ~1.1 Ga Mid-continent Rift Volcanics.

Site Information				palaeomagnetics				100% G_1^0				U/Pb Age (Ma)
		λ_s	ϕ_s	U/N	D_m	I_m	α_{95}	λ_p	ϕ_p	dp	dm	
Mid-continent rift intrusives												
ABD	Abitibi Dykes [17]	48	-81	1/20	291.9	63.1	10	44.4	211.4	12.4	15.7	1141±1 [28]
DCr	Duluth Complex R [29]	47	-92	1/13	91	-65.5	6	-33.3	44.3	7.9	9.7	1106.9±0.6, 1107.0±1.1 [20,30]
DCn	Duluth Complex N [26]	47	-92	7/97	288.6	37.2	4.1	27.6	189.5	2.8	4.8	NA
LSr	Logan Sills R [16]	49	-89	5/62	110.1	-72.1	11.2	-49.1	39.6	17.4	19.7	1108.2±0.9 [20]
TBr	Thunder Bay dykes R [31]	47.8	-89.4	1/17	112.3	-68.4	4.9	-47.6	32.1	7	8.3	NA
TBn	Thunder Bay dykes N [31]	47.8	-89.4	3/47	294.7	43	9.6	34.6	180.8	7.4	11.9	NA
Mid-continent rift extrusives												
OVr	Osler Volcanics R [5,24]	48.4	-88.6	2/37	116.1	-61	6	-45.9	18.1	7	9.2	1107.5+4/-2, 1105.3±2.1 [20,32]
Ovn	Osler Volcanics N [24]	48.4	-88.6	1/5	296.5	39.5	8.2	34	177.6	5.9	9.8	NA
lMPr	LL Mamainse Volcanics R [5,10]	47.1	-84.8	2/25	135	-70.9	8.4	-61.2	38.6	12.7	14.6	NA
lMPn	L Mamainse Volcanics N [5,10]	47.1	-84.8	2/20	290.4	41.1	7.9	30.7	187.8	5.8	9.6	NA
uMPr	U Mamainse Volcanics R [5,10]	47.1	-84.8	2/7	106.6	-56.8	13.6	-36.8	23.2	14.3	19.7	NA
uMPn	UU Mamainse Volcanics N [5,10]	47.8	-84.8	2/42	303.4	40	5.2	39	177.2	3.8	6.3	NA
NSr	L North Shore Volcanics R [5,25,33]	47.8	-89.9	3/38	120.8	-62.9	7.8	-49.8	18	9.6	12.2	1107.9±1.8, 1107.7±1.9 [20]
NSn	M North Shore Volcanics N [5,25,33]	47.5	-91	3/98	290.3	44.5	4.7	32.4	183.6	3.7	5.9	1098.4±1.9, 1096.6±1.7 [20]
CGr	L Cape Gargantua Volcanics R [5]	47.6	-85	2/11	131.6	-69	5.5	-59.1	32.4	7.9	9.3	NA
CGn	U Cape Gargantua Volcanics N [5,10]	47.6	-85	2/14	295.3	39.3	8	33.1	182.5	5.7	9.6	NA
PLr	Pillar Lake Volcanics R [34]	50.2	-89.1	1/39	108.3	-70.1	11.4	-47.7	35.0	16.9	19.6	NA
PMr	Powder Mill Volcanics R [27]	46.2	-90	1/33	97.5	-67.6	5.8	-37.9	36.9	8.1	9.7	1107.3±1.6 [20]
PLL	Portage Lake Lavas [35]	47	-88.5	1/28	291.2	31.3	5.6	26.7	178.0	3.5	6.3	1094±1.5, 1096.3±1.8 [36]
LST	Lake Shore Traps [37]	47.6	-88.1	1/20	286.1	27.5	5.9	21.5	180.2	3.5	6.4	1087.2±1.6 [36]
Kapuskasing structural zone intrusives												
CCr1	Coldwell Complex R1 [38,39]	48.8	-86.4	2/19	121	-70.9	3.3	-54.2	37	5	5.7	1108±1 [40]
CCn	Coldwell Complex R2 [39]	48.8	-86.5	1/9	119.1	-54.3	5.1	-43.8	9.5	5	7.2	NA
CCr2a	Coldwell Complex R2b [38]	48.8	-86.5	1/6	114.6	-70.5	7.1	-50.6	37.7	10.6	12.3	NA
CCr2b	Coldwell Complex N [38,39]	48.8	-86.7	2/11	301.8	60.1	5.8	49.1	195.1	6.6	8.8	NA
SCr	Shenango Complex R [41]	48.4	-83	1/9	112	-46	13	-34.4	10.9	10.6	16.6	NA
SCn	Shenango Complex N [41]	48.4	-83	1/7	304	51	10	45.1	186.4	9.1	13.5	NA
NCr	Nemegosenda Carbonatite R [41]	48	-83.1	1/4	124	-57	20	-48.6	13.8	21.2	29.1	1105.4±2.6 [21]
NCn	Nemegosenda Carbonatite N [41]	48	-83.1	2/20	312	54	13	52.2	184.1	12.8	18.2	NA

Notes: N or R at the end of the site location ID refers to normal or reversed polarities (with respect to the present local field inclination); λ_s and ϕ_s - site latitude (°N) and site longitude (°E); U/N - number of studies / sites; D_m, I_m and α_{95} - mean declination, inclination and 95% radius of confidence for palaeomagnetic direction; λ_p, ϕ_p, dp and dm - latitude, longitude and semi-minor and semi-major axes of 95% polar error ellipse assuming 100% GAD (i.e. G_1^0).

hypothesis was also favored by Robertson (1973) [10] on the basis of the presence of multiple polarity zones, not geological evidence. Detailed mapping of the Mamainse Point succession by our group and others [11,12] has not revealed evidence for the major duplicating fault postulated by Palmer and Robertson. In addition to the lack of geological evidence for faulting, elemental concentrations and neodymium isotopes measured through the sequence of basalt flows reveal trends that are not repeated, demonstrating that the basalts in each polarity zone are geochemically distinct from one another(Fig. 2b; [13,14,23]). These changes in major element, trace element, and neodymium isotopic values through the stratigraphy have been interpreted to indicate that the source of volcanism evolved throughout its eruption from a initial plume/lithospheric mantle signal to a plume/depleted mantle signal [14].

S2.3 Information and references regarding the other dual polarity localities of Keweenawan Volcanics

A summary table of other palaeomagnetic data generated from Keweenawan volcanics is included as Table S3. Some details concerning the data and geological setting from other dual polarity localities are laid out below in order to explore why data from these localities have not revealed symmetric reversals.

- In the *North Shore Volcanic group* of northern Minnesota, the older reversely magnetized basalt flows are separated from the overlying normally magnetized basalt flows by the intrusive Duluth gabbro[5,16].

- In the *Osler Group Volcanics*, as studied where it outcrops in islands in the Nipogen Strait, lower reversed flows are separated from upper normally magnetized flows by at least 0.8 km of water except on Puff Island[24]. On Puff Island, Halls (1974) studied one reversed site before a conglomerate and interpreted angular unconformity that is followed by flows of normal polarity. This one reversed site has a mean inclination (-44.2) that is quite similar to that obtained from the overlying normally magnetized flows (mean inclination of 39.5). While not definitive in any regard, such a result suggests that this area warrants further study so that the directions can be considered in a stratigraphic context, as opposed to the previous approach where all sites of each polarity are considered solely in the context of their grouped mean.

- Books (1968, 1972)[25,26] originally interpreted the lowermost flows of the Powder Mill Volcanics to be normally magnetized and to be overlain by flows of reversed magnetization. Palmer (1986)[27] revisited the succession and found that the flows have reversed magnetization to the base of the succession except in one locale of higher metamorphic grade where they argue that either later hydrothermal activity or igneous intrusions remagnetized the rocks during subsequent volcanism. The reversed flows of the Powder Mill Volcanics are separated from the younger and normally magnetized Portage Lake Volcanic group by a poorly exposed zone of felsic volcanics and clastic sedimentary rocks making the succession a difficult place to rigorously determine reversal symmetry.

- Palaeomagnetic studies of the succession of Cape Gargantua Volcanics have shown that the lower part of the stratigraphy has reverse directions of magnetizations and that sites in the upper part of the stratigraphy are normally magnetized[5,10]. To date this work has not been at high enough stratigraphic resolution for the lack of multiple reversals, or the presence of asymmetry across the known reversal, to be stated with confidence.

S2.4 Calculation for the approximation of pole velocity error

We define the polar wander velocity as v.

$$v = \frac{\Delta\theta}{\Delta t} \tag{1}$$

With $\Delta\theta$ being the minimum arc distance between two poles and Δt the difference in their U/Pb ages. The data used for this measurement of arc distance are the compilation of poles in Table S3. The error for v is calculated as below:

$$\left(\frac{\sigma_v}{v}\right)^2 = \frac{\sigma^2_{\Delta\theta}}{\Delta\theta^2} + \frac{\sigma^2_{\Delta t}}{\Delta t^2} \tag{2}$$

DOI: 10.1038/NGEO622

Table S4: Polar wander rates calculated from poles with U/Pb geochronological constraints.

	CCr	NSr	PMr	DCr	OVr	NSn	PLL
NSn	$33.6\pm3.5\,\frac{cm}{year}$	$21.7\pm6.4\,\frac{cm}{year}$	$30.3\pm4.8\,\frac{cm}{year}$	$38.5\pm4.4\,\frac{cm}{year}$	$21.5\pm7.1\,\frac{cm}{year}$		
PLL	$33.9\pm2.9\,\frac{cm}{year}$	$24.5\pm5.2\,\frac{cm}{year}$	$31.9\pm4.0\,\frac{cm}{year}$	$38.3\pm3.6\,\frac{cm}{year}$	$23.7\pm5.3\,\frac{cm}{year}$	$37.9\pm17.0\,\frac{cm}{year}$	
LST	$22.9\pm1.9\,\frac{cm}{year}$	$17.0\pm3.7\,\frac{cm}{year}$	$19.7\pm2.9\,\frac{cm}{year}$	$22.8\pm2.9\,\frac{cm}{year}$	$23.5\pm3\,\frac{cm}{year}$	$12.2\pm6.4\,\frac{cm}{year}$	$7.6\pm10.7\,\frac{cm}{year}$

The errors on the individual ages and palaeomagnetic poles are included as follows:

$$\sigma^2_{\Delta t} = \sigma^2_{\Delta t_1} + \sigma^2_{\Delta t_2} \tag{3}$$

$$\sigma^2_{\Delta\theta} = \sigma^2_{\Delta\theta_1} + \sigma^2_{\Delta\theta_2} \tag{4}$$

Solving for σ_Δ in equation 2 gives the 2σ error in °/Myr which can be converted to cm/year.

$\sigma_{\Delta\theta}$ is the angular distance of the 95% confidence error ellipse on the path that is the great circle between the two poles of interest. For intrusions (CCr and DCr) and thin packages of lava flows for which there were only single U/Pb ages (NSr, PMr, LST) the age used was the single age and $\sigma_{\Delta t}$ is the error on that age (Table S3). For volcanic units that are bound by multiple ages (OVr, NSn, PLL) we took the average of those ages and then set $\sigma_{\Delta t}$ to be large enough to encompass the error range for both ages. For example, a flow in near the base of the normal flows in the southwest limb of the North Shore Volcanic Group is dated at 1098.4 ± 1.9 Ma, while a flow near the top of the succession is dated at 1096.6 ± 1.7 Ma. Taking the average of the two ages gives us 1097.5, and we assign it a $\sigma_{\Delta t}$ of 2.8 Ma to encompass the 95% confidence range of the two ages.

Calculations of polar wander velocities and their approximated errors are shown in Table S4.

S2.5 Comments on the "Logan Loop"

While it remains the best resolved Precambrian polar wander path, the "Logan Loop" can be improved by pairing U-Pb ages with a more nuanced approach to palaeomagnetic poles. While the averaging out of secular variation does require the use of many individual flow VGPs when calculating a pole, the current data sets necessitate the practice of taking the mean of palaeomagnetic data from a polarity chron or formation and assigning it to a single age or multiple ages from the flows/intrusions. This procedure is necessary because the palaeomagnetic data is not generated from the same site or immediate stratigraphic sections as the geochronological data. Pairing geochronological data to paleomagnetic data on the formation level reduces the resolution that could potentially exist for the APW curve. Removing the need to invoke substantial non-GAD components at the time of the Logan Loop allows us to focus on its behaviour as a record of continental motion, as opposed to an artefact of an unusual geomagnetic field.

S2.6 The relationship between the Umkondo and Keweenawan igneous provinces

Exactly coeval with the early volcanism in the Keweenawan rift was the development of the Umkondo igneous province in the Kalahari craton[42]. Like the Keweenawan rift, this igneous province developed inland from a 1.1 Ga orogenic belt–the Namaqua-Natal Belt[42]. The synchroneity of the volcanism and similar tectonic setting has lead to speculation that Laurentia and Kalahari were adjacent and that the volcanism was sourced by a single mantle plume[43]. However, when mean paleomagnetic poles from the two igneous provinces are calculated with a GAD assumption and compared, they imply a minimum separation of ~2400 km. With the flexibility that would be inherent through invoking significant non-dipole components to explain the purported Keweenawan reversal asymmetry, this separation could be entirely removed. For

example, with a 0.27*GAD quadrupole contribution to the surface geomagnetic field, Kalahari could be situated next to northeast Laurentia. This is one of many examples of how paleogeographic reconstructions for the late Mesoproterozoic can be significantly effected by invoking substantial non-dipole contributions to the field and demonstrates why Keweenawan reversal symmetry is commonly referenced as a concern in paleogeographic reconstructions. The discovery that the 3 reversals at Mamainse Point are symmetric shows that reversal asymmetry is not present in the Keweenawan volcanics. This result mitigates the need for concern about the validity of Mesoproterozoic paleogeographies that are reconstructed assuming 100% GAD. This leaves us with the result of Hanson (2004)[42] that despite the fact that Kalahari and Laurentia both had outboard active collisional margins and coeval volcanism at 1.1 Ga they were >2000 km apart.

S2.7 More background on challenges to the GAD hypothesis through Earth History

The GAD hypothesis has been challenged for both the Palaeozoic and Proterozoic eras. Van der Voo and Torsik (2001)[44] proposed a 10% octupole model to explain discrepancies between geological and palaeomagnetic observations related to the reconstruction of Pangaea from 250-300 Ma. Further analysis by Van der Voo and Torsik, however, led them to conclude that the low-latitude bias that would be imparted by an octupole component could be, and likely is, a result of misassigned ages to poles and inclination shallowing in sedimentary rocks[45]. Bloxham (2000)[46] used a numerical geodynamo model to show that the evolution of lateral heat-flux variations at the core-mantle boundary could generate sustained axial octupoles. Since the pattern of heat flux across the core-mantle boundary has likely changed through geologic time, the fact that the last 150 Ma is consistent with the GAD hypothesis does not guarantee that such a field dominated in the more distant past.

Kent and Smethurst (1998) used compilations of the frequency distribution of palaeomagnetic inclinations throughout Earth history to argue that shallow inclinations are over-represented for the Palaeozoic and Precambrian eras[47]. They interpreted this reported predominance of low inclination data as possibly a result of a geomagnetic field that contained a 25% octupole component at the Earth's surface. These results were challenged by Meert et al. (2003),[48] who showed that the current paleomagnetic database is not sufficient to test the GAD model and that the data as binned by Kent and Smethurst (1998)[47] can not provide a robust statistical test for a GAD distribution. Furthermore, Meert et al. (2003) demonstrated that non-GAD-like distributions can readily be produced through insufficient sampling and argued that the results of inclination-only data compilations are currently ineffective means to evaluate for the presence of non-dipole fields.

The interpretation that the low-latitude bias in Precambrian palaeomagnetic data is a result of long-lived non-GAD components to the geomagnetic field conflicts with the compiled evaporite palaeolatitude results[49], which indicate that there was no substantial and long-lived octupolar component to the Precambrian field. If low-latitude bias is a true feature of the paleomagnetic record and not a result of incomplete sampling, it could alternatively be explained as a result of the tendency of continents to be driven to low latitudes through true polar wander during supercontinent cycles[47,50].

DOI: 10.1038/NGEO622

References

[1] Kirschvink, J. The least-squares line and plane and the analysis of paleomagnetic data. *Geophysical Journal of the Royal Astronomical Society* **62**(3), 699–718 (1980).

[2] Halgedahl, S. and Jarrard, R. Low-temperature behavior of single-domain through multidomain magnetite. *Earth and Planetary Science Letters* **130**, 127–139 (1995).

[3] Dunlop, D. and Argyle, K. Separating multidomain and single-domain-like remanences in pseudo-single-domain magnetites (215-540 nm) by low temperature demagnetization. *Journal of Geophysical Research* **96**, 2007–2017 (1991).

[4] Cogne, J. P. PaleoMac: A Macintosh (TM) application for treating paleomagnetic data and making plate reconstructions *Geochemistry, Geophysics, Geosystems* **4**, 1007 (2003).

[5] Palmer, H. Paleomagnetism and correlation of some Middle Keweenawan rocks, Lake Superior. *Canadian Journal of Earth Science* **7**, 1410–1436 (1970).

[6] Merrill, R. T. and Grommé, C. S. Nonreproducible self-reversal of magnetization in diorite. *Journal of Geophysical Research* **74**, 2014–2024, April (1969).

[7] Palmer, H., Halls, H., and Pesonen, L. Remagnetization in Keweenawan rocks. Part I: conglomerates. *Canadian Journal of Earth Science* **18**, 599–618 (1981).

[8] Jones, C. User-driven integrated software lives: "PaleoMag" paleomagnetics analysis on the Macintosh. *Computers and Geosciences* **28**, 1145–1151 (2002).

[9] Tauxe, L., Bertram, H., and Seberino, C. Physical interpretation of hysteresis loops: Micromagnetic modeling of fine particle magnetite. *Geochemistry, Geophysics, Geosystems* **37**(10), 1–22 (2002).

[10] Robertson, W. Pole positions from the Mamainse Point Lavas and their Bearing on a Keweenawan pole path. *Canadian Journal of Earth Science* **10**, 1541–1555 (1973).

[11] Annells, R. Proterozoic flood basalts of eastern Lake Superior: the Keweenawan volcanic rocks of the Mamainse Point area, Ontario. *Geological Survey of Canada Paper* **72-10** (1973).

[12] Giblin, P. E. Kincaid Township. *Preliminary Geological Map, Ontario Department of Mines* **553** (1969).

[13] Massey, N. Keweenawan paleomagnetic reversals at Mamainse Point, Ontario: fault repitition or three reversals? *Canadian Journal of Earth Science* **163**, 373–375 (1979).

[14] Shirey, S., Klewin, K., Berg, J., and Carlson, R. Temporal changes in the sources of flood basalts: isotopic and trace element evidence for the 1100 Ma old Keweenawan Mamainse Point Formation, Ontario, Canada. *Geochimica Cosmochimicha Acta* **58**, 4475–4490 (1994).

[15] Dubois, P. Paleomagnetism and correlation of Keweenawan rocks. *Bulletin of the Geological Survey of Canada* **71**, 1–75 (1962).

[16] Halls, H. and Pesonen, L. Paleomagnetism of Keweenawan rocks. *Geological Society of America Memoirs* **156**, 173–201 (1982).

[17] Ernst, R. and Buchan, K. Paleomagnetism of the Abitibi dike swarm, souther Superior Province, and implications for the Logan Loop. *Canadian Journal of Earth Science* **30**, 1886–1897 (1993).

[18] Schmidt, P. W. and Williams, G. E. Reversal asymmetry in Mesoproterozoic overprinting of the 1.88-Ga Gunflint Formation, Ontario, Canada: non-dipole effects or apparent polar wander? *Tectonophysics* **377**(1-2), 7–32 (2003).

[19] Davis, D., Green, J., and Manson, M. Geochronology of the 1.1 Ga North American Mid-Continent Rift. In *Program and Abstracts*. Institute on Lake Superior Geology, (1995).

[20] Davis, D. and Green, J. Geochronology of the North American Midcontinent rift in western Lake Superior and implications for its geodynamic evolution. *Canadian Journal of Earth Science* **34**, 476–488 (1997).

[21] Heaman, L., R.M., E., Hart, T., Hollings, P., MacDonald, C., and Smyk, M. Further refinement to the timing of Mesoproterozoic magmatism, Lake Nipogon region, Ontario. *Canadian Journal of Earth Science* **44**, 1055–1086 (2007).

[22] Davis, D. Personal communication. email (2007).

[23] Klewin, K. and Berg, J. Geochemistry of the Mamainse Point volcanics, Ontario, and implications for the Keweenawan paleomagnetic record. *Canadian Journal of Earth Science* **27**, 1194–1199 (1990).

[24] Halls, H. A paleomagnetic reversal in the Osler Volcanic Group, northern Lake Superior. *Canadian Journal of Earth Science* **11**, 1200–1207 (1974).

[25] Books, K. Magnetization of the lowermost Keweenawan lava flows in the Lake Superior area, Geological Survey research 1968, chapter D. *U.S. Geological Survey Professional Paper* **P 0600-D**, 248–254 (1968).

[26] Books, K. Paleomagnetism of some Lake Superior Keweenawan rocks. *U.S. Geological Survey Professional Paper* **P 0760**, 42 (1972).

[27] Palmer, H. and Halls, H. Paleomagnetism of the Powder Mill Group, Michigan and Wisconsin; a reassessment of the Logan Loop. *Journal of Geophysical Research* **91**(B), 11,571–11,580 (1986).

[28] Krogh, T., Corfu, F., Davis, D., Dunning, G., Heaman, L., Kamo, S., Machado, N., Greenough, J., and Nakamura, E. Precise U-Pb isotopic ages of diabase dykes and mafic to ultramafic rocks using trace amounts of baddeleyite and zircon. In Mafic dyke swarms, Halls, H. and Fahrig, W., editors, volume 34. Geological Association of Canada (1987).

[29] Beck, M. Paleomagnetism of Keweenawan intrusive rocks, Minnesota. *Journal of Geophysical Research* **75**(26), 4985–4996 (1970).

[30] Paces, J. and Miller, J. Precise U-Pb ages of Duluth Complex and related mafic intrusions, northeastern Minnesota: geochronological insights to physical, petrogenetic, paleomagnetic and tectonomagmatic processes associated with the 1.1 Ga Midcontinent Rift system. *Journal of Geophysical Research* **98**, 13997–14013 (1993).

[31] Pesonen, L. Paleomagnetism of late Precambrian Keweenawan igneous and baked contact rocks from Thunder Bay district, northern Lake Superior. *Bulletin of the Geological Society of Finland* **51**, 27–44 (1979).

[32] Davis, D. and Sutcliffe, R. U-Pb ages from the Nipigon plate and northern Lake Superior. *Geological Society of America Bulletin* **96**, 1572–1579 (1985).

[33] Hubbard, H. Keweenawan geology of the Porcupine mountains, western Upper Peninsula, Michigan. *Proceedings and Abstracts - Institute on Lake Superior Geology, Annual Meeting* **17**, (1971).

[34] Borradaile, G. and Middleton, R. Proterozoic paleomagnetism in the Nipigon Embayment of northern Ontario: Pillar Lake Lava, Waweig Troctolite and Gunflint Formation tuffs. *Precambrian Research* **144**, 69–91 (2006).

[35] Hnat, J. S., van der Pluijm, B. A., and Van der Voo, R. Primary curvature in the Mid-Continent Rift: Paleomagnetism of the Portage Lake Volcanics (northern Michigan, USA). *Tectonophysics* **425**, 71–82, (2006).

[36] Davis, D. and Paces, J. Time resolution of geologic events on the Keeweenaw Peninsula and applications for development of the Midcontinent Rift system. *Earth and Planetary Science Letters* **97**, 54–64 (1990).

DOI: 10.1038/NGEO622

[37] Diehl, J. and Haig, T. A paleomagnetic study of the lava flows within the Copper Harbour Conglomerate, Michigan: new results and implications. *Canadian Journal of Earth Sciences* **31**, 369–380 (1994).

[38] Robertson, W. Paleomagnetism of the 1.1 Ga Coldwell Complex. unpublished (1970).

[39] Lewchuk, M. and Symons, D. Paleomagnetism of the Clay-Howells Carbonatite Complex: constraints on Proterozoic motion in the Kapuskasing Structural Zone, Superior Province, Canada. *Tectonophysics* **172**, 67–75 (1990).

[40] Heaman, L. and Machado, N. Timing and origin of midcontinent rift alkaline magmatism, North America: evidence from the Coldwell Complex. *Contributions to Mineralogy and Petrology* **110**, 289–303 (1992).

[41] Costanzo-Alvarez, V., Dunlop, D., and Pesonen, L. Paleomagnetism of alkaline complexes and remagnetization in the Kapuskasing Structural Zone, Ontario, Canada. *Journal of Geophysical Research* **98**(B3), 4063–4079 (1993).

[42] Hanson, R., Crowley, J., Bowring, S., Ramezani, J., Gose, W., Dalziel, I., Pancake, J., Seidel, E., Blenkinsop, T., and Mukwakwami, J. Coeval large-scale magmatism in the Kalahari and Laurentian Cratons during Rodinia assembly. *Science* **304**, 1126–1129 (2004).

[43] Hanson, R., Martin, M., Bowring, S., and Munyanyiwa, H. U-Pb zircon age for the Umkondo dolerites, eastern Zimbabwe: 1.1 Ga large igneous province in southern Africa-East Antarctica and possible Rodinia correlations. *Geology* **26**, 1143–1146 (1998).

[44] Van der Voo, R. and Torsvik, T. Evidence for late Paleozoic and Mesozoic non-dipole fields provides an explanation for the Pangea reconstruction problems. *Earth and Planetary Science Letters* **187**, 71–81 (2001).

[45] Van der Voo, R. and Torsvik, T. The quality of the European Permo-Triassic paleopoles and its impact on Pangea reconstructions. In Timescales of the paleomagnetic field, Channell, J., Kent, D., Lowrie, W., and Meert, J., editors, volume 145 of *Geophysical Monograph*. American Geophysical Union (2004).

[46] Bloxham, J. Sensitivity of the geomagnetic axial dipole to thermal core-mantle interactions. *Nature* **405**, 63–65 (2000).

[47] Kent, D. and Smethurst, M. Shallow bias of paleomagnetic inclinations in the Paleozoic and Precambrian. *Earth and Planetary Science Letters* **160**, 391–402 (1998).

[48] Meert, J. G., Tamrat, E., and Spearman, J. Non-dipole fields and inclination bias: insights from a random walk analysis. *Earth and Planetary Science Letters* **214**, 395–408, 9 (2003).

[49] Evans, D. Proterozoic low orbital obliquity and axial-dipolar geomagnetic field from evaporite palaeolatitudes. *Nature* **444**, 51–55 (2006).

[50] Evans, D. True polar wander, a supercontinental legacy. *Earth and Planetary Science Letters* **157**, 1–8 (1998).

PALAEOMAGNETISM

In GAD we trust

Palaeomagnetists' basic assumption that Earth's magnetic field is a GAD, that is, a geocentric axial dipole, has been challenged by anomalous magnetic data from ancient Canadian basalts. At a closer look, fast continental drift could explain this anomaly.

Joseph G. Meert

Reconstructing the position of the land masses on the globe through deep time is like completing a blank puzzle. Palaeogeographers have only the known outlines of the continents and a few palaeomagnetic data to help them estimate past latitude and orientation of the land masses. To make matters worse, the palaeomagnetic data can be contradictory, and it can be difficult to unravel the many signals contained within a limited study. In the case of the 1.1-billion-year-old Keweenawan rocks of the Canadian shield, attempts to reconstruct the position of North America have been muddled, as the palaeomagnetic data have been controversially interpreted to reflect a deviation of Earth's magnetic field from the basic assumption of a geocentric axial dipole (GAD) model[1,2,3]. On page 713 of this issue, Swanson-Hysell and colleagues look at the rocks in higher resolution and neatly lay to rest the long-standing controversy over the nature of Earth's magnetic field 1.1 billion years ago[4].

Magnetic minerals in rocks — particularly those formed from molten rock — will align with the magnetic field. Rocks found today thus record the magnetic field direction at the time of their solidification. These palaeomagnetic data can aid the reconstruction of the movements of the continents, but only if the Earth's magnetic field is known sufficiently well. Palaeomagnetism therefore relies on the fundamental assumption that the Earth's magnetic field behaves as a GAD, that is, essentially as if there were a bar magnet centred in the Earth's core and aligned with the axis along which the Earth spins, giving rise to normal or reverse polarity (Fig. 1a,b). A more complex magnetic field and reversals (Fig. 1c) will introduce errors in palaeogeographic reconstructions. Evidence from the past few million years shows that the Earth's magnetic field is indistinguishable from the GAD model[5], but the structure of the field earlier in Earth's history is more controversial[4].

The Earth's magnetic field has periodically reversed polarity through time[6]. According to the GAD model, a shift from a normal (north-seeking) to a reverse (south-seeking) magnetic field will result in a change in the sign of the inclination, that is, the angle the magnetic field lines make with the surface of the globe; this angle varies with latitude from 0° at the Equator to 90° at the poles. Furthermore, the declination (the angle between the local magnetic north and geographic north) would be exactly 180° opposed. However, if more poles were present and remained stationary during reversal of the axial field, such as depicted in Fig. 1c, there would be large asymmetry in normal and reverse polarity directions, making it nearly impossible to produce reliable palaeogeographic maps.

Such reversal asymmetry has been suggested for the latter part of the Mesoproterozoic (~1.1 billion years ago)[1,2]. During this time, much of the continental crust was aggregating into a supercontinent

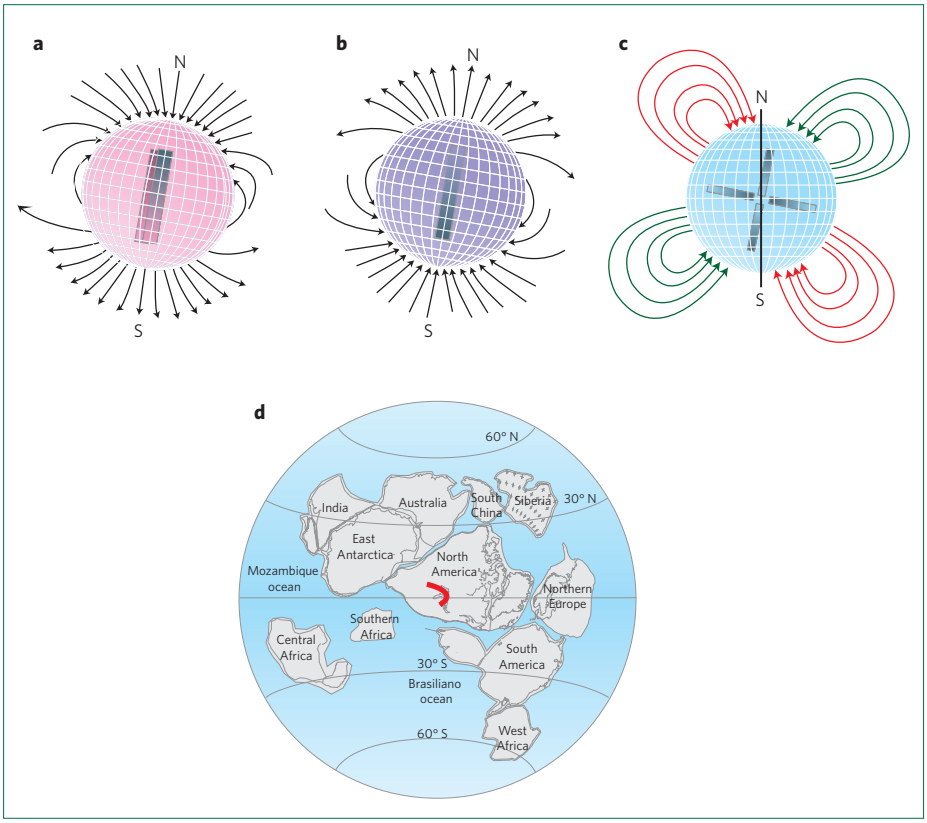

Figure 1 | Magnetic reversals and their records. **a**,**b**, Assuming a geocentric axial dipole magnetic field under normal (**a**) or reverse (**b**) polarity, the field behaves as if there were a bar magnet centred in the Earth and aligned with the spin axis. **c**, To explain the Keweenawan rocks of the Canadian shield, it has been proposed that the field can behave as a non-axial quadrupole field[5,6]. **d**, The supercontinent Rodinia formed about one billion years ago. Previous studies from the Keweenawan basalts (shown in red) suggested that reversals during this time had a non-axial quadrupole component (**c**). Swanson-Hysell and colleagues demonstrate[4] that the reversals recorded in the basalts were actually symmetric; the appearance of asymmetry in averaged normal and reverse directions arose from aliasing effects of recording the rapid motion of North America with low-resolution palaeomagnetic data.

known as Rodinia[7,8] (Fig. 1d). At the same time, a large volume of basaltic material erupted in the middle of the existing North American continent. Palaeomagnetic studies of these volcanic rocks, known as the Keweenawan basalts, have revealed a remarkable asymmetry between the inclinations observed in the average 'normal' polarity samples and the average 'reverse' polarity samples[1,2].

As the rocks were thought to have erupted over a relatively short time interval, the authors of those studies argued that this asymmetry indicates a significant deviation from the GAD model. They suggested that the structure of the Earth's magnetic field included a large contribution from a non-GAD field[1,2], which remained stationary while the GAD field underwent a symmetric reversal.

Swanson-Hysell and colleagues took a closer look at the reversal structure in the Keweenawan basalts at Mamainse Point near Lake Superior[4]. The lava pile at Mamainse is thick (~4,500 m) and contains several sequences of reverse and normal polarity magnetization. More importantly, the authors noted that each of the sequences of normal and reversed polarity were separated from the next by a time gap, when basalt was not flowing to the surface. Swanson-Hysell and colleagues obtained similar palaeomagnetic results to the earlier studies[1,2], but offer an alternative explanation for the asymmetry between the normal and reverse directions. They argue that the past studies, which simply averaged all normal and reverse directions, were flawed because North America underwent significant latitudinal motion, much of which was not recorded because of the gaps in volcanic activity. When averages of normal and reverse polarity directions are taken from lavas of the same age within the sequence, the directions perfectly fit the GAD model. According to these new observations, the apparent asymmetry is not due to any long-standing anomalous field behaviour, but instead to the rapid latitudinal motion of North America.

This conclusion explains the root cause of the asymmetry, but it requires unusually fast continental motion. Large continents generally move over the Earth at rates of less than 5 cm yr^{-1}. The rates proposed in this study are four to seven times higher. Swanson-Hysell and colleagues hint that this rapid motion was a response to mass instabilities in the mantle. In their model, the instability caused the entire crust and mantle to move rapidly to a dynamically stable configuration. This process, called true polar wander, repositions the excess mass (in this instance North America) towards the Equator.

The beauty of the true polar wander hypothesis is that it can be tested, as long as high-resolution data, similar to those reported here, exist for other continents. Indeed, there is some indication of true polar wander during the time interval in question from existing studies[4,7], although further work is needed to confirm this hypothesis.

Swanson-Hysell and colleagues have provided a new model[4] for explaining the magnetic field data from the Keweenawan rocks without the need for any non-GAD field contribution. If they are right, palaeomagnetists can henceforth conduct palaeogeographic reconstructions without worrying about a capricious magnetic field. ❐

Joseph G. Meert is at the Department of Geological Sciences at the University of Florida, Gainesville, Florida 32611, USA.
e-mail: jmeert@ufl.edu

References

1. Pesonen, L. & Nevanlinna, H. *Nature* **294,** 436–439 (1981).
2. Nevanlinna, H. & Pesonen, L. *J. Geophys. Res.* **88,** 645–658 (1983).
3. Gallet, Y., Pavlov, V., Semikhatov, M. & Petrov, P. *J. Geophys. Res.* **105,** 16481–16499 (2000).
4. Swanson-Hysell, N. L., Maloof, A. C., Weiss, B. P. & Evans, D. A. D. *Nature Geosci.* **2,** 713–717 (2009).
5. McElhinny, M., McFadden, P. & Merrill, R. *J. Geophys. Res.* **101,** 25007–25027 (1996).
6. Opdyke, N. D. & Channell, J. E. T. *Magnetic Stratigraphy* (International Geophysics Series Vol. 64, Academic Press, 1996).
7. Meert, J. G. & Torsvik, T. H. *Tectonophysics* **375,** 261–288 (2003).
8. Li, Z. X. *et al. Precambrian Res.* **160,** 179–210 (2008).

BIOGEOCHEMISTRY

Fire's black legacy

Forest fires convert a small portion of burning vegetation into charred solid residues such as charcoal. A survey of Scandinavian forest soils reveals that charcoal has a highly patchy distribution, and a shorter-than-expected lifetime.

Caroline M. Preston

Millions of hectares of boreal forest — coniferous forest in the high latitude Northern Hemisphere — are burnt each year, mostly in unmanaged sparsely populated regions[1]. The twentieth century has seen a rise in boreal forest fires, which in Canada has been linked to rising summer temperatures[2]. The risk of fire — together with the area burnt — is predicted to increase by at least twofold in Canada, Alaska and Russia by 2100 (refs 1,3,4), with potential ramifications for the global carbon cycle. A small portion of forest fuel is converted into solid charred residues[5,6] such as char, charcoal, soot and graphite — termed black carbon. These residues are considered to be highly resistant to decomposition, and are therefore thought to function as a long-term carbon sink. However, despite their significance, the distribution and turnover time of the pyrogenic carbon pool is poorly constrained. On page 692 of this issue, Ohlson and colleagues present results from an exhaustive survey of soil charcoal in Scandinavian forests, and show that the abundance and carbon content of charcoal varies through space and time[7].

Forest fires convert the majority of burning vegetation and soil organic matter into carbon dioxide, emitting around 250 Tg (1 Tg = 10^{12} g) of carbon per year in the pan-boreal forest alone[8]. However, approximately 1–3% of the burning organic matter gets converted into black carbon. Black carbon has a complex molecular structure, which is thought to increase its resistance to microbial decomposition — indeed, the lifetime of soil black carbon is known to extend to thousands of years[5,6,9].

However, recent research suggests that the amount of black carbon in boreal forest soils is lower than that predicted based on fire frequency and presumed lifetimes. Thus, the soil black-carbon pool may be less resistant to breakdown than previously thought. Equally uncertain is the size of the soil black-carbon sink: although black-carbon residues have been found in soils across the globe, the size of this